NAA-SR-12355

THERMAL BEHAVIOR OF SNAP 8 REACTOR DURING ATMOSPHERIC REENTRY

AEC Research and Development Report

ATOMICS INTERNATIONAL
A DIVISION OF NORTH AMERICAN AVIATION, INC.

DISCLAIMER

Printed in the United States of America
Available from
Clearinghouse for Federal Scientific and Technical Information
National Bureau of Standards, U.S. Department of Commerce
Springfield, Virginia 22151
Price: Printed Copy $3.00; Microfiche $0.65

NAA-SR-12355
AEROSPACE SAFETY

THERMAL BEHAVIOR OF SNAP 8 REACTOR DURING ATMOSPHERIC REENTRY

By

L. D. MONTGOMERY
J. E. ARNOLD
E. M. MOURADIAN
D. K. NELSON

ATOMICS INTERNATIONAL

A DIVISION OF NORTH AMERICAN AVIATION, INC.

CONTRACT: AT(04-3)-701
ISSUED: MAY 1, 1967

DISTRIBUTION

This report has been distributed according to the category Aerospace Safety as given in the Standard Distribution for Unclassified Scientific and Technical Reports, TID-4500. The edition used was the one currently in effect on the date this document was issued.

CONTENTS

TABLES

FIGURES

FIGURES

FIGURES

ABSTRACT

An analysis was carried out to simulate the thermal behavior of a SNAP-8 type reactor system during reentry into the earth's atmosphere. The objective of this analysis was to determine whether sufficient ablation will occur to release the reactor core at an altitude that will insure complete burnup of the fuel elements in the upper atmosphere.

From the results of this analysis, it is concluded that the SNAP-8 reactor vessel will not ablate to a sufficient extent, for probable modes of reentry, to release the fuel elements at altitudes necessary to obtain complete fuel ablation.

I. INTRODUCTION

An analysis was carried out to simulate the thermal behavior of a SNAP-8 type reactor system during reentry to the earth's atmosphere. The objective of this analysis was to determine whether sufficient ablation will occur to release the reactor core at an altitude that will insure complete burnup of the fuel elements in the upper atmosphere. This work was conducted as a portion of the overall Aerospace Nuclear Safety Program.

The general sequence of events which the system must undergo is the melting off or removal of the upper head portion of the reactor system, breakup of the reactor core by melting open the vessel wall or melting off the grid plate, ablation and breakup of the fuel elements, burnup of fuel elements, and dispersal of the remaining fine particles into the upper atmosphere. The successful completion of this sequence of events is dependent upon reactor core release from the reentering system. Of particular interest is the aerodynamic heating generated by the reentering body and its thermal effect upon reactor top head and vessel wall.

In this report, the term "top head," or upper head, denotes the upper lid of the reactor core and the forward NaK piping. The term "reactor core" denotes the bundle of 211 fuel elements, the internal reflectors, and the two grid plates. The "vessel wall" is the SS-316 vessel which houses the reactor core components.

The analysis presented in this report concerns the heating and subsequent removal of the reactor's top heat and vessel wall during two modes of reentry. During the first mode of reentry investigated, the reactor system was assumed to be fastened to the neutron shadow shield assembly, and to be spinning about its axis. Three cases were investigated for this mode; 0°, 30°, and 70° angles of attack. The "angle of attack" is the angle formed by the line of flight and the longitudinal axis of the system. Although the angle of attack does not stay constant during reentry, the three cases investigated were based on the assumption of constant angles of attack so as to determine the relative effect on thermal behavior.

Under the second mode of reentry, the reactor was assumed to be released from the shield at an altitude of 400,000 ft followed by random tumbling into the earth's atmosphere.

The most probable mode of reactor breakup is not certain. In this analysis, the assumption was made that as the system reenters, direct aerodynamics heating occurs on the upper head and vessel wall, the only portion actually exposed to the flow stream. During the first phase of the flight, heating of the internal portions of the system takes place only indirectly; that is, by internal conduction and radiation. Eventually, sufficient heating will have occurred to melt-through portions of the top head or vessel wall, exposing the internal core components to direct aerodynamics heating.

The actual mode of reactor system breakup and core component release is not immediately evident. It would occur either as a result of melting away of the top head, or ablation of the vessel wall surrounding the fuel elements. Results of this analysis indicate that the mode of reentry and the angle of attack largely determine which of the two portions actually melts away on the reentering system.

II. REFERENCE REENTRY TRAJECTORY

The RESTORE (Reentering SNAP Trajectory on an Oblate Rotating Earth) computer program was used to calculate the trajectory of the reentering system. The trajectory depends on the body's ballistic coefficient, as well as on its initial velocity, position, and orientation. In order to determine these aerodynamic coefficients, an approximation of the reactor-shield assembly geometry was made, and is shown in Figure 1. The drag coefficient acting on a body of the configuration as shown in figure, was determined by the NEWTON Code. The NEWTON Code is a computer program formulated to evaluate the force and moment coefficients on axisymmetric bodies in hypersonic flow based on NEWTONIAN flow theory. The results of the NEWTON Code calculations are shown in Figure 2. It is evident that for a wide range of angles of attack (0° to 90°) The drag coefficient varies only slightly (C_D = 1.00 ± 0.04), from which it follows that the ballistic coefficient ($W/C_D A_{ref}$ lbm/ft^2) also varies only about 4%.

This justifies using the same reentry trajectory for all angles of attack between head-on (α = 0°) and side-on (α = 90°) orientation. Accordingly, the

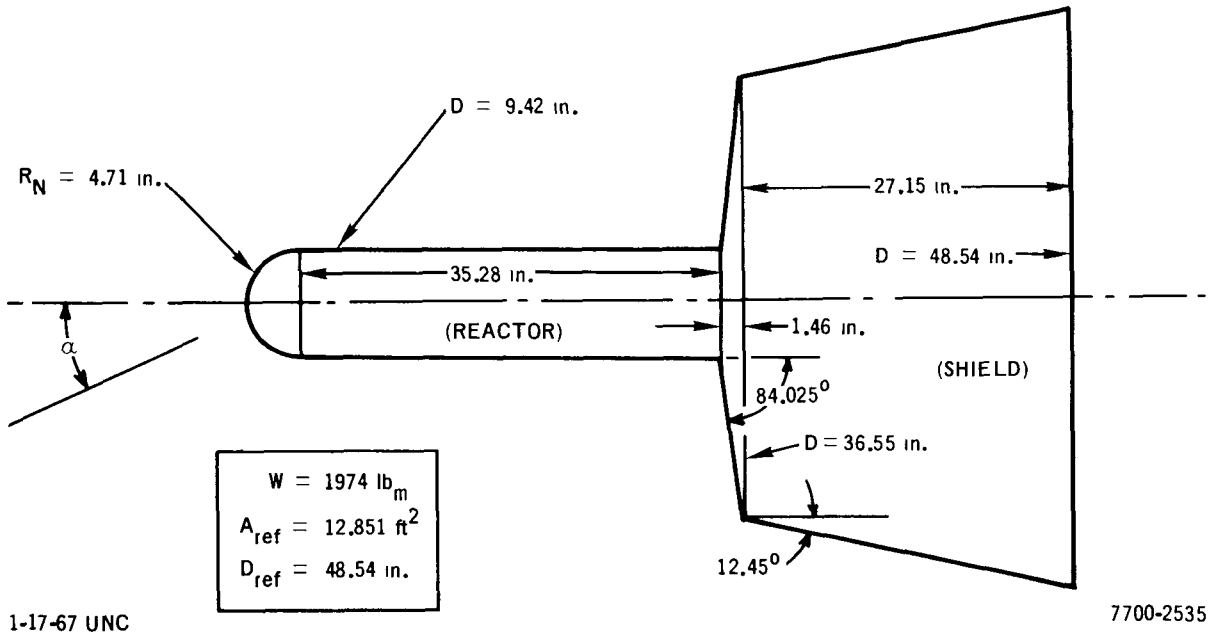

Figure 1. Assumed Reentry Geometry of Reactor-Shield Assembly

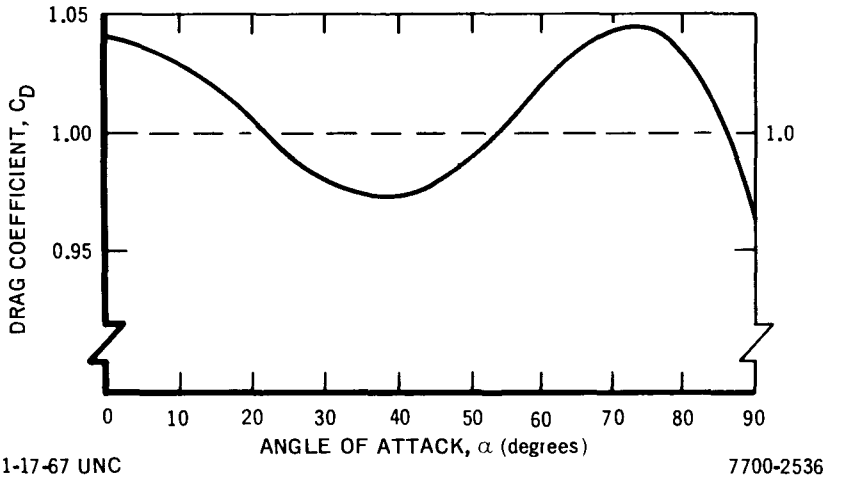

Figure 2. Drag Coefficient vs Angle of Attack for Reference Geometry of Reentry Vehicle

ballistic coefficient value of $W/C_D A_{ref} \cong 1.53$ lbm/ft^2 was used throughout the first mode of reentry cases.

A variable $C_D A$ coefficient was used in the RESTORE calculation to determine the trajectory of the system during the second mode of reentry. The weight, W, of the system was taken to be the weight of the NaK void SNAP-8 reactor without the neutron shadow shield. During this trajectory calculation the reactor was assumed to be detached from the shield at 400,000 ft.

Among the trajectory parameters determined by the RESTORE Code are the altitude, velocity, flight angle, longitude, latitude, azimuth, and range as a function of time. As a side calculation, the code also computes the nominal reference heating, q_{ref}, which is:

$$q_{ref} \frac{\text{Btu}}{\text{sec-ft}^2} = 865 \sqrt{\frac{\rho}{\rho_{SL}}} \left(\frac{V}{V_o}\right)^{3.15}$$

as given by Detra and Hidalgo (see Reference 1) as the stagnation point heating on a sphere with a 1-ft radius. (V_o is the reference velocity of 10,000 ft/sec and ρ_{SL} is the air density at sea level.)

The results of the RESTORE Code calculations are shown for the reference trajectories in Figures 3 and 4. The solid traces in Figure 3 indicate the system's altitude and reference heating rate vs time, with the reactor attached to the neutron shadow shield. The dashed traces in Figure 3 show the altitude and reference heating rate vs time for the SNAP-8 reactor released from the shadow shield at 400,000 ft under the second mode of reentry considered. Figure 4 gives the reference heating vs altitude for the reactor-shield system during reentry (solid trace), and the reactor-random tumbling case (dashed trace).

The actual aerodynamic heating on any point on the reentering system is given by the expression:

$$Q_N \frac{\text{Btu}}{\text{sec}} = (q_{ref}) \underbrace{\left[\sqrt{\frac{R_o}{R}} \frac{q_{\text{local (radius = R)}}}{q_{\substack{\text{stag} \\ \text{sphere}}} \text{ (radius = R)}} \right]}_{\varphi} (\text{HWCR}) \, A_N.$$

The hot-wall correction factor, (HWCR), has been neglected in the calculations reported herein, as it is consistently close to unity. The heat-loading factor, φ, is made up of the size correction factor, $\sqrt{R_o/R}$, and the location factor, $q_{local}/q_{stag\ sphere}$. The local heat-loading factors, φ, as applied to the given calculations, were acquired from the aeroheating test conducted at Cornell Aeronautical Laboratories and the RADE tests. These experiments are discussed in the appendices of this report. The local heat-loading factors, φ, as applied to the thermal model presented in this report, are discussed in detail in Section V.

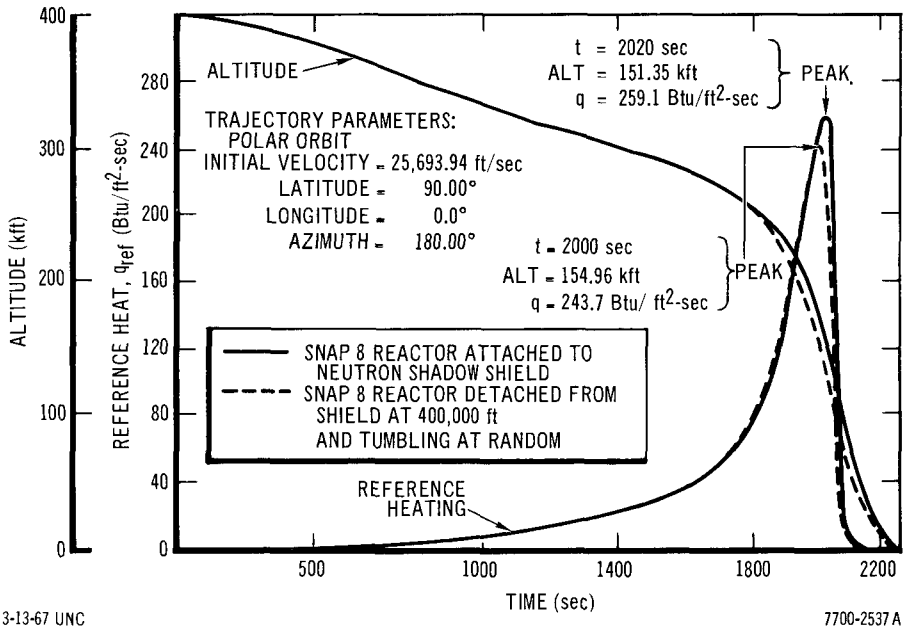

Figure 3. Altitude and Reference Heating vs Time for Reference Trajectories

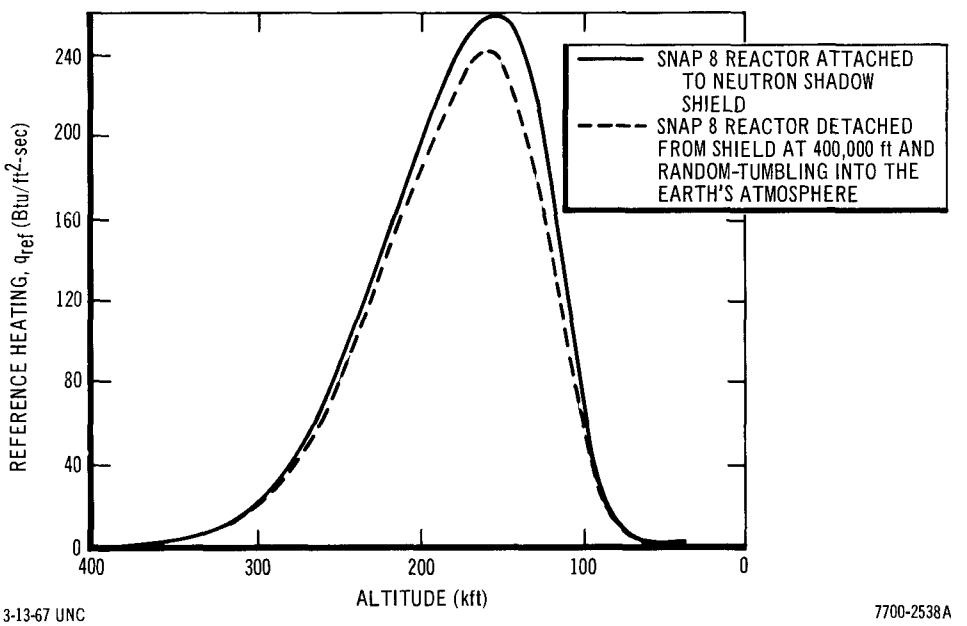

Figure 4. Reference Heating vs Altitude for Reference Trajectories

III. GEOMETRIC AND THERMAL PROPERTIES OF SNAP SYSTEM

The geometric configuration and dimensions of the SNAP-8 reactor core, vessel, and top head were simulated by the analytical model. In describing the geometry of the core for trajectory and thermal calculations, design parameters were followed, though some approximations were assumed for computational simplicity. Only axial and radial variations of geometric parameters were taken into account. No circumferential variable was considered. Thus, in the nodal division used in the thermal model, the grid plate and fuel elements were handled as annuli. The grid plate and fuel elements were treated as nine concentric regions, one central circle, and weighted successive rings. See Section IV on the nodal model for details of system geometry.

The reactor system is composed primarily of Type 316 stainless steel, uranium-zirconium hydride fuel material, and lesser quantities of beryllium and Hastelloy C and Hastelloy N. The material properties used in the thermal analysis are given in Table 1. Thermal properties for beryllium and Hastelloy are not listed. These materials occur in such small portions in the reactor that they were not considered separately. The beryllium was lumped with the fuel, and the Hastelloy with the stainless steel.

Thermal properties of the stainless steel and fuel materials were assumed to be constant.

TABLE 1

THERMOPHYSICAL PROPERTIES OF MATERIALS

Stainless Steel – 316	
Thermal Conductivity, K,	4.7×10^{-4} Btu/in-°F-sec
Density, ρ,	0.286 lbm/in^3
Thermal Capacity, C_p,	0.18 Btu/lbm-°F
Thermal Emissivity, ε,	0.7
Fuel Material	
Thermal Conductivity, K,	5.0×10^{-4} Btu/in-°F-sec
Density, ρ,	0.22 lbm/in^3
Thermal Capacity, C_p	0.2 Btu/lbm-°F
Thermal Emissivity, ε,	0.4

IV. ANALYTICAL MODEL OF SNAP-8 REACTOR

In order to investigate the thermal behavior of the reentering reactor system, an analytical model was developed to represent the constituent portions of the system. This analytical model was devised for use with the "Thermal Analyzer Program" (TAP), computer code.

The TAP Code carries out the solution of transient or steady-state problems in heat transfer where the system to be analyzed is described by means of a set of conductances, capacitances, etc, in the manner of the electrical thermal analog.

The modes and paths of heat transfer on the model were represented by (thermal) resistors set up to represent radiation heat transfer as well as conduction. Structural members (thermal capacity) were represented by nodes and capacitors. This analytical model permitted detailed simulation of the SNAP-8 reactor.

The top head portion of the analytical model represents the upper lid, or upper head of the reactor vessel, and a portion of the NaK outlet pipe extending above the vessel. The portion of the SNAP-8 system simulated by the top head portion of the analytical model was assumed to be at the front during reentry for the cases considered. The upper head encloses the reactor core within the vessel, and must be removed before the reactor upper grid plate can be exposed to direct aerodynamic heating.

Figure 5 shows the node division, radiation heat exchange paths, and conductance network for the top head portion of the analytical model.

The reactor core and vessel portion of the analytical model represents the reactor fuel elements, internal beryllium reflectors, the grid plates and the reactor vessel. The analytical model represents the total length of the reactor but is more detailed (smaller nodal sections) in the forward portion of the reactor core. The temperature information of most interest and significance occurs near the front (or top) of the reactor core. Figure 6 illustrates the reactor core and vessel portion of the analytical model.

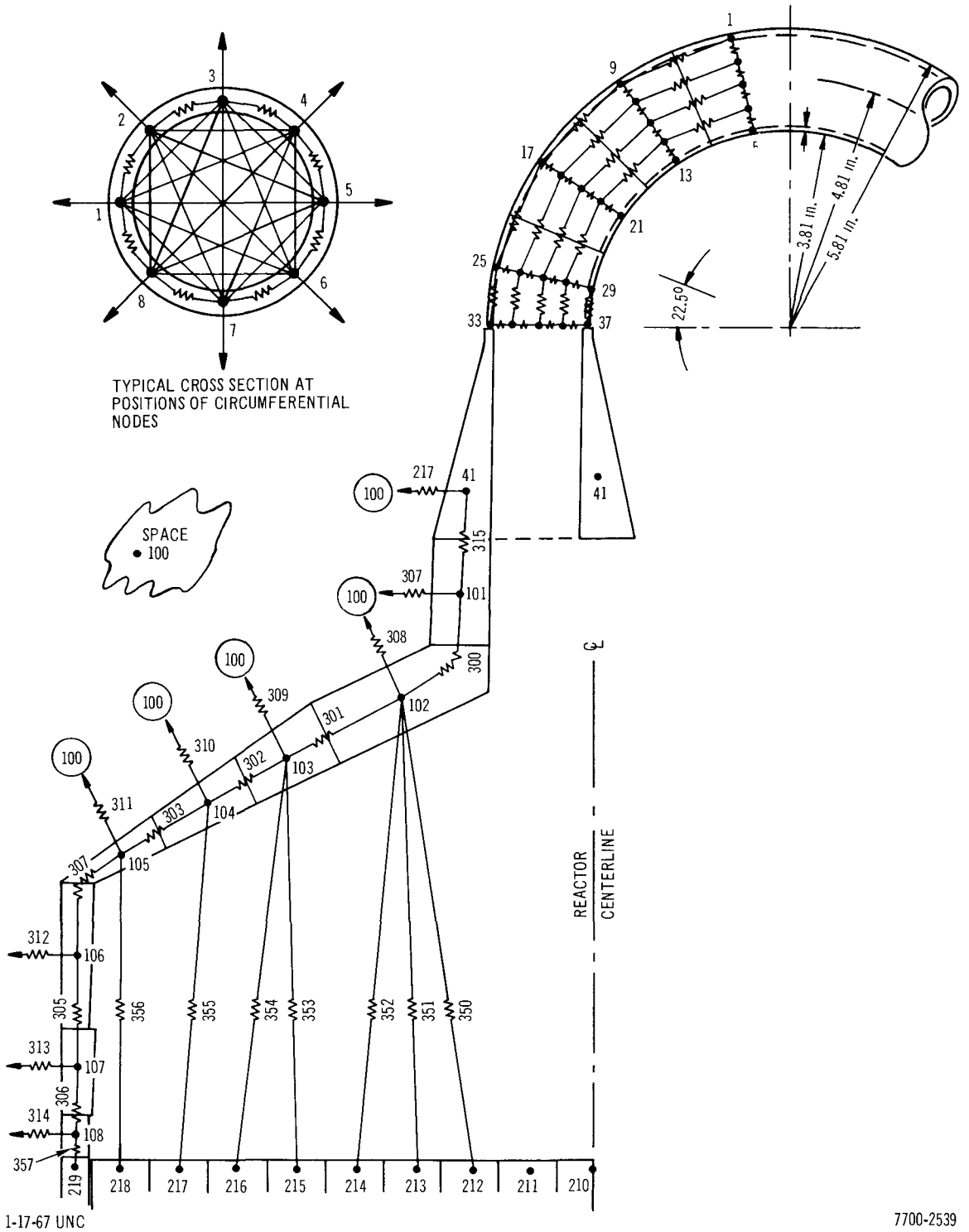

Figure 5. Nodal Network of Top Head (and NaK Pipe) Thermal Model

BLANK

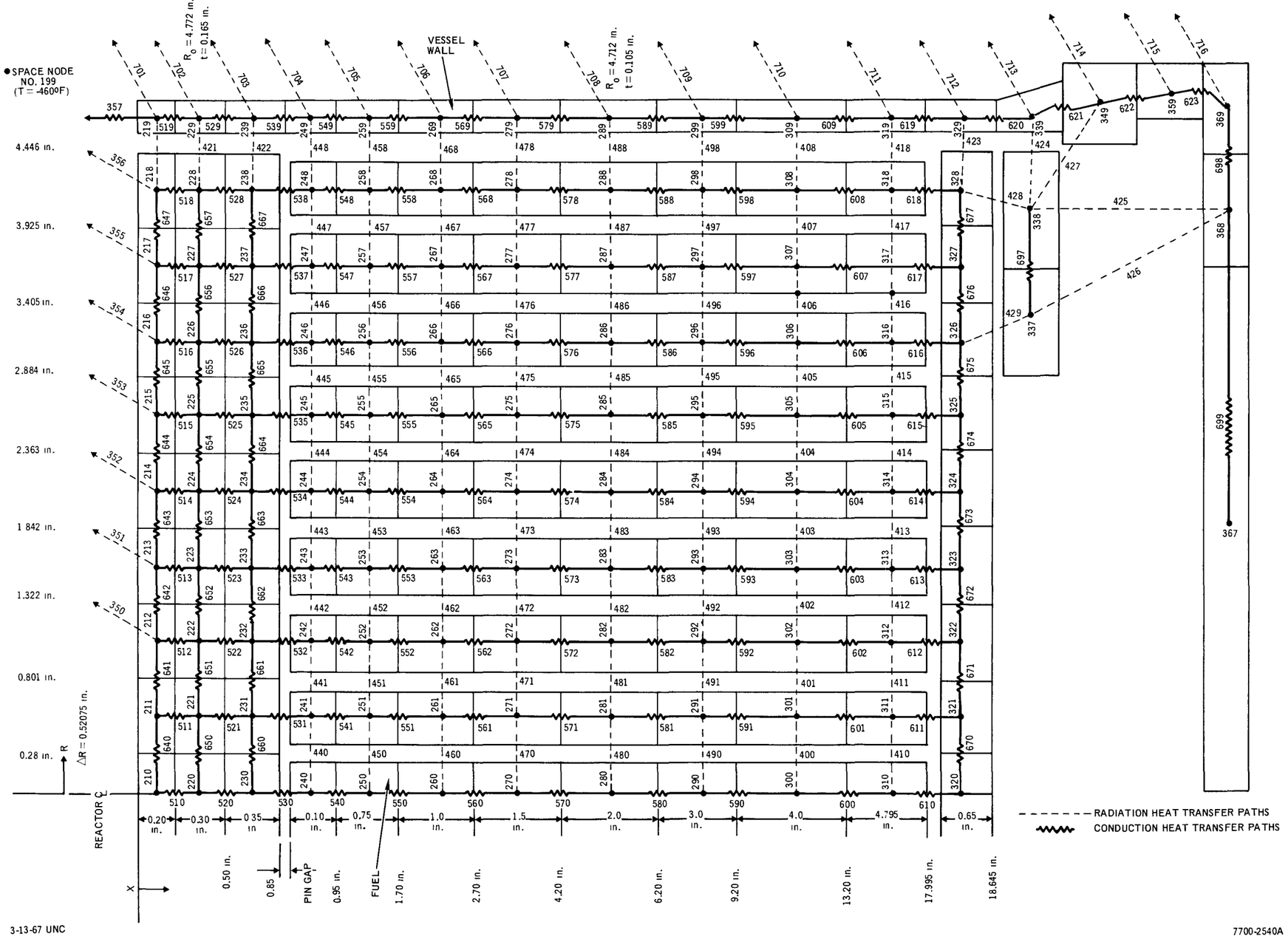

Figure 6. Nodal Network of Reactor Core and Vessel Model

BLANK

TAP models similar to the one used in this analysis were used to calculate the experimental temperature response of the RADE ablation models during the RADE experiment. (See Appendix B). Good correlation was obtained between the analytical calculations and the RADE experimental results. In this way, the RADE experiment demonstrated the accuracy of the analytical techniques used to predict the preablation thermal behavior of the SNAP-8 reactor upon reentry to the earth's atmosphere.

In devising the reactor core and vessel portion of the analytical model, longitudinal and radial variations of temperature were taken into account, but circumferential variations were neglected. Thus, an annular model of the core and vessel was set up. The upper grid plate was divided into nine radial portions, a central section with a 0.28-in. radius, and eight concentric annuli with ΔR's (ΔR = 0.52075 in.) to the outer radius of the grid plate, 4.446 in.

The actual SNAP-8 upper grid plate has holes drilled through it in an axial direction. The presence of these holes was not directly accounted for in setting up the nodal model. In determining the capacitances and conductances of the grid plate nodal network, the grid plate was treated as a solid plate, and the following corrections were made. The nodal masses and axial conductances were corrected by the factor,

$$\frac{\rho'}{\rho_o} = \frac{K'}{K_o} = \frac{\text{gross volume of grid plate} - \text{volume of holes}}{\text{gross volume of grid plate}} = \left(1 - \frac{\text{void}}{\text{fraction}}\right) = 0.723.$$

The radial conductances were corrected by the factor,

$$\left(\frac{K'}{K_o}\right)_{\text{radial}} = \frac{1 - \text{void fraction}}{1 + \frac{\text{void fraction}}{3}} = 0.662$$

This expression for the lateral thermal conductivity in a perforated solid is given by Jakob.[2]

The fuel elements were also treated as annuli. The fuel elements are placed in the core roughly in the pattern of concentric rings. Therefore, the fuel was

represented by nine concentric regions in the analytical model. The center region represents the center fuel element, and the other eight represent succeeding rings of fuel elements, with the outer ring including the internal beryllium reflector.

Volumes and cross-sectional areas of nodes representing the fuel elements were based on the number of fuel elements located in each ring, as Table 2 shows. Radial heat transfer between fuel element rings was assumed to be by radiation only.

TABLE 2
FUEL ELEMENTS IN NODAL RINGS

Ring No.	No. of Elements
0	1
1	6
2	12
3	18
4	24
5	30
6	36
7	42
8	48*
9	Vessel wall

*Includes 42 fuel elements plus 6 "equivalent" reflector rods.

Radiation heat rejection from the surface of the reactor system to outer space (at $T_{space} = -460°F$) was with a surface emissivity, $\epsilon = 0.7$, and unity view factor. Aerodynamic heating was applied to the surface nodes.

No provision was made in the thermal model to handle the melting phenomenon. The model was set up so that the nodes continued to increase in temperature until a temperature of 2800°F was reached. At this temperature, a given node is no longer iterated by the computer code. In assessing the computer output, a temperature of 2800°F is taken as signifying melting. Stainless steel has a melting temperature of approximately 2600°F. In taking 2800°F as the melting temperature, a ΔT of 200°F above the melting temperature of the stainless steel has been allowed to account for the latent heat. The latent heat of the metal compared to the specific heat is quite high, such that a ΔT of 500 to 1000°F is required to approximate the enthalpy of the latent heat of fusion. On the other hand, melting of the stainless steel may have to occur only partially, to weaken the material so much that it no longer can hold together.

When the "melting temperature" of an alloy is reached, melting starts in the grain boundaries, since the lower melting constituents tend to collect there.

The result is that an alloy will lose all its strength much more quickly than a pure substance when melting starts, because it tends to break up along the grain boundaries. This would indicate that, in order to destroy a portion of the reactor, it may not be necessary to supply the entire "latent heat" to melt it away but merely a relatively small amount of heat to initiate the melting at the grain boundaries.

When the stainless steel is in a heated and weakened condition, portions of the top head or vessel wall may break away or be torn off by aerodynamic shear stresses or bearing stresses of the core components on the reactor vessel.

V. AERODYNAMIC HEAT LOADING

The basic aerodynamic heating relationship used in making the calculations reported herein was the Detra-Hidalgo correlation;

$$q_{ref}\left(\frac{Btu}{sec\text{-}ft^2}\right) = q_{\substack{SS \\ sphere \\ stag \\ point}} = 865\sqrt{\frac{R_o}{R}}\sqrt{\frac{\rho}{\rho_{SL}}}\left(\frac{V}{V_o}\right)^{3.15}\left(\frac{H_{stag} - H_{wall}}{H_{stag} - H_{T=540°R}}\right) \quad \ldots(1)$$

which is presented in Reference 2. Equation 1 is for the stagnation point heating on a sphere of radius, R, and velocity, V, in flight through air of density, ρ. The terms R_o, ρ_{SL}, and V_o are reference parameters. The reference radius, R_o, is 12 in., the reference velocity, V_o, is 10,000 ft/sec; and the reference air density, ρ_{SL}, is that of standard air at sea level, 0.07647 lbm/ft^3.

The final term of the Detra-Hidalgo expression is called the "hot-wall correction factor," and accounts for the fact that the higher the temperature of a surface, the less heat will flow to it from the heat source. In the work presented in this report, the hot-wall correction has been neglected. Trajectory calculations indicated that until the very final stages of the flight, the stagnation enthalpy is so high as to make the hot-wall correction very close to unity.

The size correction factor, $\sqrt{R_o/R}$, is the ratio stagnation point heating on a sphere of radius R to the stagnation point heating on a sphere with a radius of 12 in. (R_o).

The aerodynamic heating on the surface of the reentering body under the first mode of reentry is expressed by

$$q_{\substack{local \\ stag\ line}}\left(\frac{Btu}{sec}\right) = q_{\substack{sphere\ stag \\ point\ R=12}}\underbrace{\left(\frac{q_{\substack{sphere\ stag \\ point\ R=R}}}{q_{\substack{sphere\ stag \\ point\ R=12}}}\right)\left(\frac{q_{\substack{local \\ (various\ shapes) \\ (R=R)}}}{q_{\substack{sphere\ stag \\ point\ R=R}}}\right)}_{\varphi = \left(\frac{q_{local\ (R=R)}}{q_{\substack{sphere\ stag \\ point\ (R=12)}}}\right)} A_N \quad \ldots(2)$$

where

$$q_{\substack{\text{sphere stag}\\ \text{point } R=12}} = q_{ref}\left(\frac{\text{Btu}}{\text{ft}^2\text{-sec}}\right) = 865\sqrt{\frac{\rho}{\rho_{SL}}}\left(\frac{V}{V_o}\right)^{3.15} \quad \text{Reference heating}$$

$$\left(\frac{q_{\substack{\text{sphere stag}\\ \text{point } R=R}}}{q_{\substack{\text{sphere stag}\\ \text{point } R=12}}}\right) = \sqrt{\frac{R_o}{R}} = \begin{matrix}\text{Size}\\ \text{correction}\\ \text{factor}\end{matrix}$$

and

$$\left(\frac{q_{\substack{\text{local}\\ \text{(various shapes)}\\ R=R}}}{q_{\substack{\text{sphere stag}\\ \text{point } R=R}}}\right) = \begin{matrix}\text{Local heating factor}\\ \text{for geometry in question,}\\ \text{to be experimentally}\\ \text{determined and corrected}\\ \text{for mode of reentry}\end{matrix}$$

and A_N is the nodal surface area in ft^2.

The local heating factors on the SNAP-8 system for the three angles of attack considered under the first mode of reentry were taken from the results of the Aeroheating Tests conducted at the Cornell Aeronautical Laboratory (see Appendix B), and the RADE Experiment (see Appendix A). The values of (q_{local}/ $q_{\text{sphere stag point } R=R}$) along the stagnation heating line of the SNAP-8 reactor were further corrected to account for system rotation for the 30 and 70° angle-of-attack cases. To average the heat input around the surface of the rotating system the stagnation-line heat rates were multiplied by $0.36 = q_{average}/q_{\text{local stag line}}$.[3]

To obtain the average local heat input to a given node on the reactor under the second mode of reentry, the q_{local} values given by Equation 2 were multiplied by $0.28 = q_{average}/q_{\text{local stag line } R=R}$.[3] The 0.28 factor corrected the heat input rates to account for random tumbling of the system during reentry.

The values of the experimentally determined and rotation-corrected local heating factors, $q_{\text{local (various shapes) } R=R}/q_{\text{sphere stag point } R=R}$, used in

the 0°, 30°, and 70° angle of attack cases under the first mode of reentry are given in Table 3. Nodal numbers in Table 3 refer to the locations on the analytical model (see Figures 5 and 6), to which the corresponding heat factors were applied. These factors were obtained from the Cornell Aeroheating experiment and are explained in the results section of Appendix B.

TABLE 3

EXPERIMENTALLY DETERMINED AND ROTATIONAL-CORRECTED LOCAL HEATING FACTORS USED IN THE 0°, 30°, AND 70° ANGLE OF ATTACK CASES UNDER THE FIRST MODE OF REENTRY

Node	0° Experiment q_1/q_{stag}	30° Experiment q_1/q_{stag}	Corrected for Rotation	70° Experiment q_1/q_{stag}	Corrected for Rotation
41	0.982	0.763	0.273	0.980	0.351
101	1.110	0.832	0.298	0.780	0.279
102	1.240	0.860	0.308	0.630	0.226
103	1.220	0.645	0.231	0.680	0.243
104	1.20	0.536	0.192	0.710	0.254
105	0.765	0.485	0.174	0.722	0.258
106	0.125	0.405	0.145	0.742	0.266
107	0.80	0.350	0.125	0.755	0.270
108	0.80	0.305	0.109	0.768	0.275
219	0.085	0.267	0.096	0.753	0.270
229	0.084	0.262	0.094	0.742	0.266
239	0.083	0.255	0.091	0.726	0.260
249	0.083	0.255	0.091	0.726	0.260
259	0.0805	0.240	0.086	0.683	0.244
269	0.078	0.227	0.081	0.652	0.233
279	0.073	0.231	0.083	0.638	0.228
289	0.066	0.238	0.085	0.610	0.218
299	0.055	0.246	0.088	0.575	0.206
309	0.047	0.255	0.091	0.548	0.196
319	0.047	0.363	0.129	0.603	0.216
329	0.0475	0.418	0.150	0.634	0.227
339	0.0455	0.375	0.134	0.663	0.237
349	0.0415	0.255	0.091	0.768	0.275
359	0.0380	0.223	0.080	0.845	0.303
369	0.0380	0.223	0.080	0.845	0.303

VI. RESULTS

A. CASES WITH REACTOR ATTACHED TO SHADOW SHIELD

Three angles-of-attack were considered under this mode of reentry: 0°, 30°, and 70°. Initial conditions of these calculations, at the start of reentry, were as follows; time = 0 sec, altitude = 400,000 ft, and temperature = 0°F. During these calculations, it was assumed that the reentering system was spinning about its axis so that there was no circumferential variation of aerodynamic heat loading.

1. 0° Angle-of-Attack Case

Temperatures of representative portions of the SNAP-8 system are shown as functions of time in Figure 7, for the 0° angle-of-attack case. The locations of the respective nodes plotted in Figure 7 are shown in Figures 5 and 6. The number designation and approximate location of the nodal temperatures shown in Figure 7 are as follows.

Node No.	Location
1	Top-center, leading edge of NaK outlet pipe
5	Bottom-center, trailing edge of NaK outlet pipe
17	~56° center, leading edge of NaK outlet pipe
21	~56° center, trailing edge of NaK outlet pipe
41	Base of NaK outlet pipe
104	Top portion of upper head
106	Side portion of upper head
219	Top of vessel wall adjacent to upper grid plate
220	Center of upper grid plate
300	Center fuel element halfway between grid plates
309	Middle of vessel wall
359	Base of reactor vessel adjacent to shadow shield

Initial ablation of the forward portion of the NaK out-let pipe occurred at 1245 sec, 311,000 ft altitude. The leading edge of the NaK outlet pipe is fully ablated by 1670 sec, 276,000 ft altitude. The base of the NaK outlet pipe (Node 41) ablates at 1880 sec, 234,000 ft. When the base of the NaK outlet pipe melts

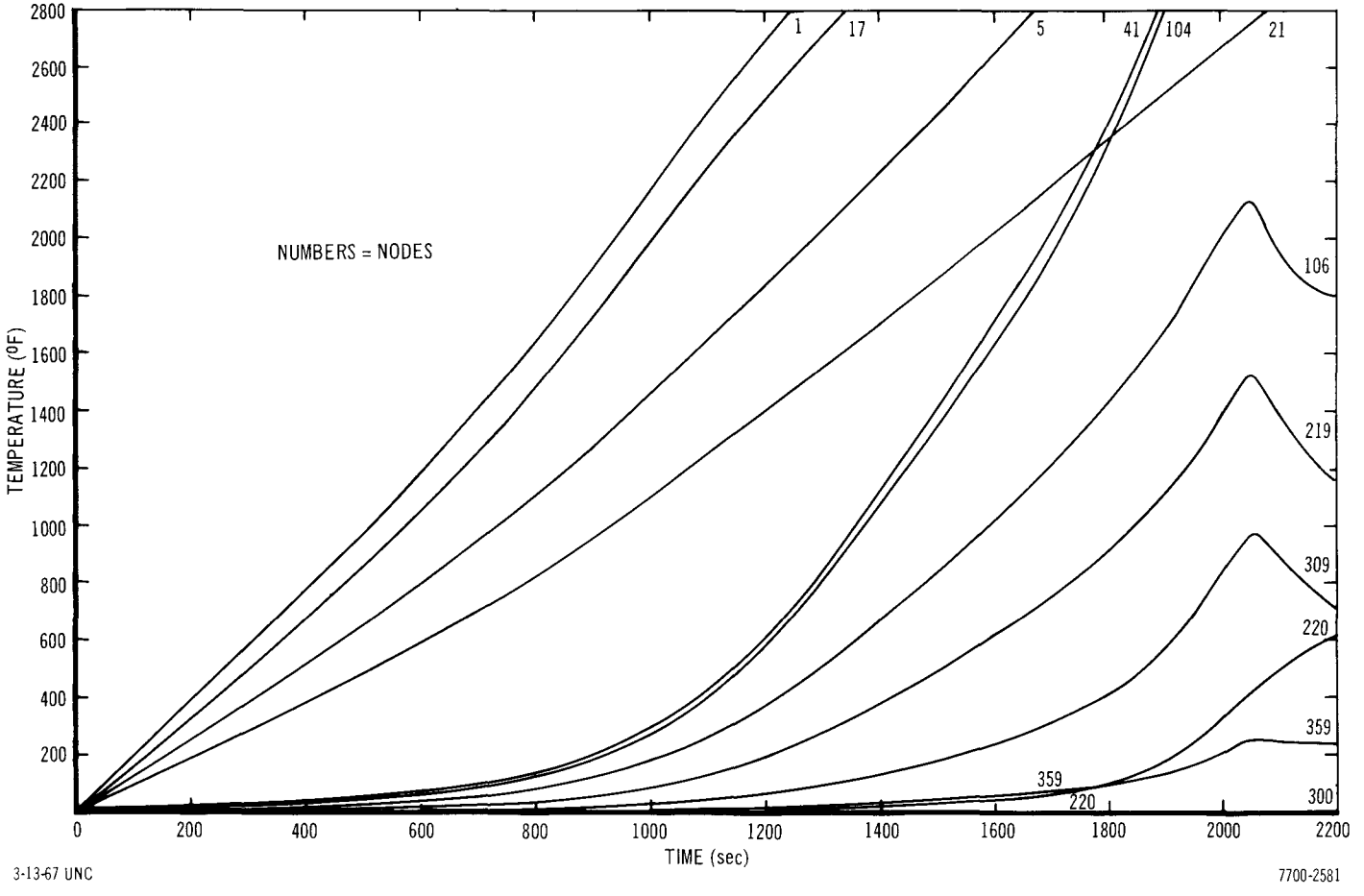

Figure 7. Temperatures of Representative Portions of SNAP-8 Reactor (0° Angle-of-Attack)

through and falls off, the remaining, trailing edge portion of the NaK pipe goes with it. Initial ablation of the top head takes place at Node 104 at 1900 sec, 226,000 ft altitude. By the time of peak heating, 2020 sec. 151,000 ft altitude, the upper portion of the top head has ablated. At this time, the vertical portions of the top head (Nodes 106 to 108) have not ablated and are at temperatures of 2120 to 1590°F, respectively. The reactor vessel wall varies in temperature from 1520°F opposite the upper grid plate to 250°F at the base of the reactor. Internal fuel temperatures remain quite low, 10 to 450°F, depending upon location. The outside ring of fuel elements varies in temperature from 450°F under the upper grid plate, and 106°F halfway between grid plates, to 38°F next to the lower grid plate. The center fuel element is 250°F under the upper grid plate, 18°F halfway between grid plates, and ~2°F next to the lower grid plate. Upper grid plate temperatures are in the 300 to 800°F range.

Radial temperature profiles for various axial positions in the reactor core, at the time and altitude of peak heating, are shown in Figure 8. The temperature profiles illustrated in Figure 8 are normalized to the outside radius of the SNAP-8 reactor vessel. These temperature profiles show the influence of the three modes of heat transfer into the reactor core: (1) radiation heat transfer from the heated vessel wall to the outer rings of fuel elements; (2) radiation heat transfer from the reactor's top head to the upper grid plate; and (3) axial conductive heat transfer from the upper grid plate to the fuel elements. The sharp increase in temperature in the outer two rings of fuel and the vessel wall is caused by the first mode of heat transfer. The decrease in temperature toward the reactor center line may be explained by Figure 5. The center portion of the upper grid plate receives no radiant heat transfer from the top head. This portion of the reactor core is directly below the NaK outlet pipe and therefore was not connected to the top head by radiant heat transfer paths in the analytical model. This temperature decrease may be overemphasized in the analytical model as compared to that in the actual case. The reactor portion of the upper grid plate will actually receive radiant heat from those portions of the top head that are not directly overhead. The uniform decrease in temperature at progressive positions into the reactor core and the damping out of the ununiform temperature distribution evident at the top surface of the upper grid plate is caused by the third mode of heat transfer mentioned above.

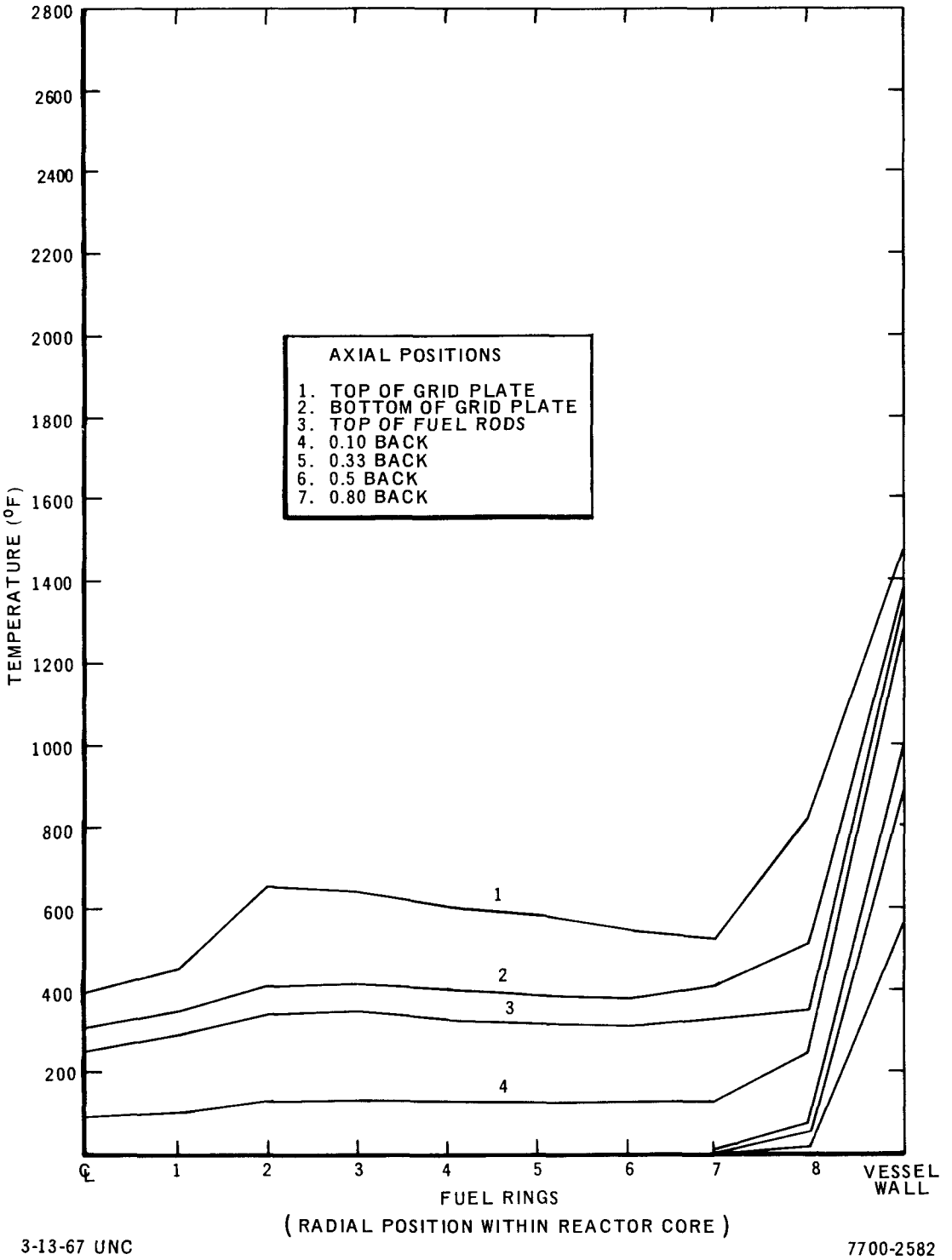

Figure 8. Radial Temperature Profiles of SNAP-8 Reactor (0° Angle-of-Attack, at Time and Altitude of Peak Heating)

2. 30° Angle-of-Attack Case

To shorten the computer time required for each calculation, the NaK outlet pipe portion of the analytical model was omitted from the 30 and 70° angle-of-attack cases. From the results of the 0° angle-of-attack case, it was felt that the NaK outlet pipe will initially ablate for each angle-of-attack considered. The complete removal of the NaK outlet pipe and the opening of the reactor core to direct aerodynamic heating are both dependent upon ablation of the top head portion of the SNAP-8 system. This aspect of the reentry disintegration sequence can be accurately investigated with the NaK outlet pipe deleted from the analytical model. The temperatures of the same portions (excluding those on the NaK outlet pipe) of the SNAP-8 reactor as shown in Figure 7 are given for the 30°F angle-of-attack case in Figure 9. By plotting the temperatures of the same portions of the reactor for each reentry case, a basis of comparison is formed to determine the relative affect of increasing angle-of-attack.

The base of the NaK outlet pipe (Node 41) initially ablates at 1940 sec, 209,000 ft altitude. Initial ablation of the reactor's top head occurs at Node 104 at 2000 sec, 169,000 ft altitude. The top head continues to ablate and is completely melted by time and altitude of peak heating, 2020 sec, 151,000 ft. At this time, the vessel wall adjacent to the upper grid plate (Node 219) is 2255°F. The central portion of the vessel wall (Node 309) is ~2040°F, and the base of the reactor vessel (Node 359) is 1390°F.

The interior temperatures of the reactor core are similar to those which occurred during the 0° angle-of-attack case. Radial temperature profiles, taken at the same axial positions as for the 0° case, are given in Figure 10. As shown in Figure 10, the vessel wall and outer ring of fuel elements attain a much higher temperature during the 30° angle-of-attack case than that reached during head-on reentry. This may be attributed to the increased aerodynamic heat loading on the reactor's vessel as the angle-of-attack increases.

Also evident in Figure 10 is the fact that the central and lower portions of the vessel reach higher temperatures than the upper regions of the reactor vessel. During the Cornell aeroheating experiment it was found that the neutron shadow shield creates a shock wave that interacts with the shock pattern produced by the reactor's top head to increase the aerodynamic heat loading to the

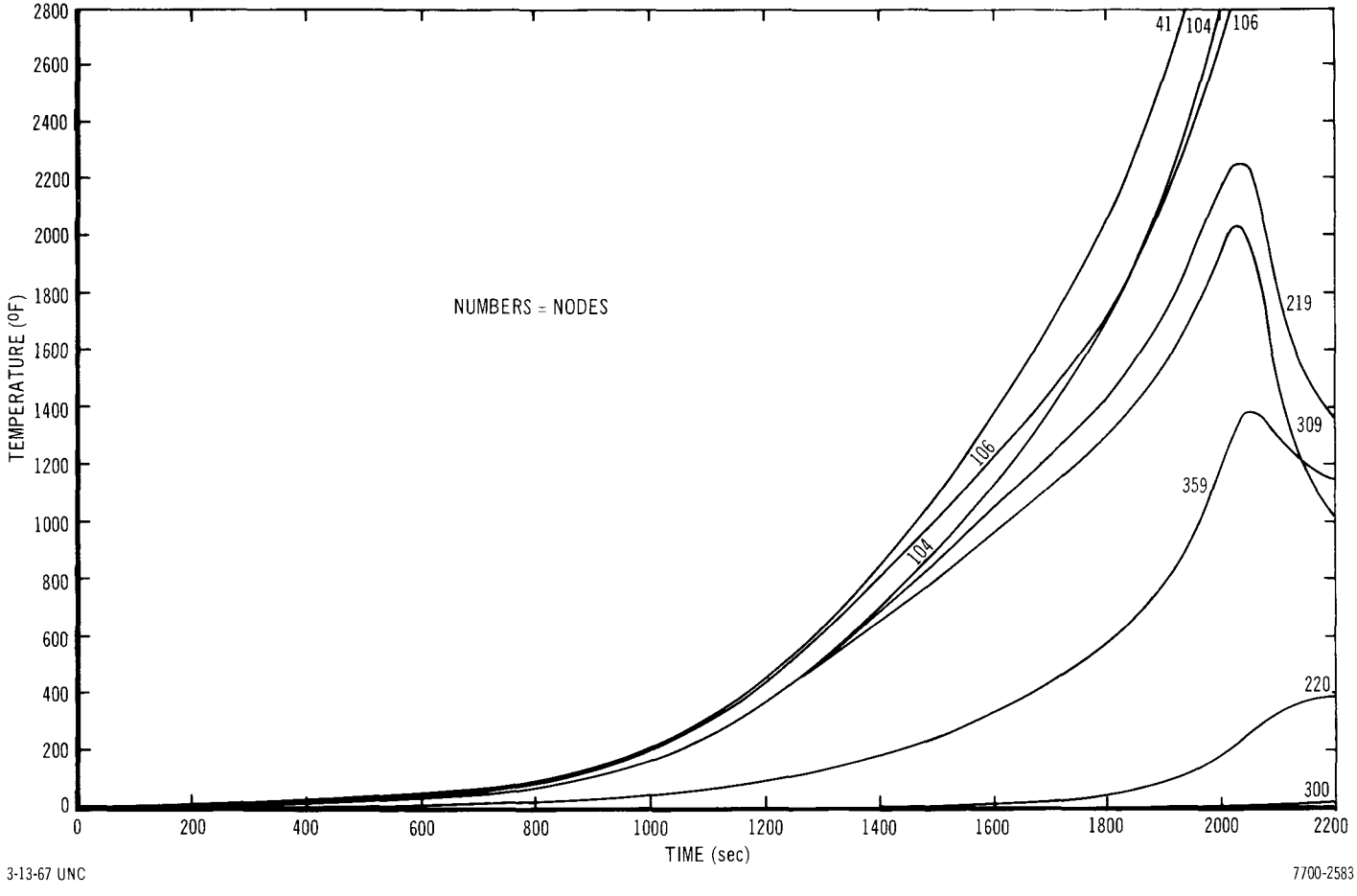

Figure 9. Temperatures of Representative Portions of SNAP-8 Reactor (30° Angle-of-Attack)

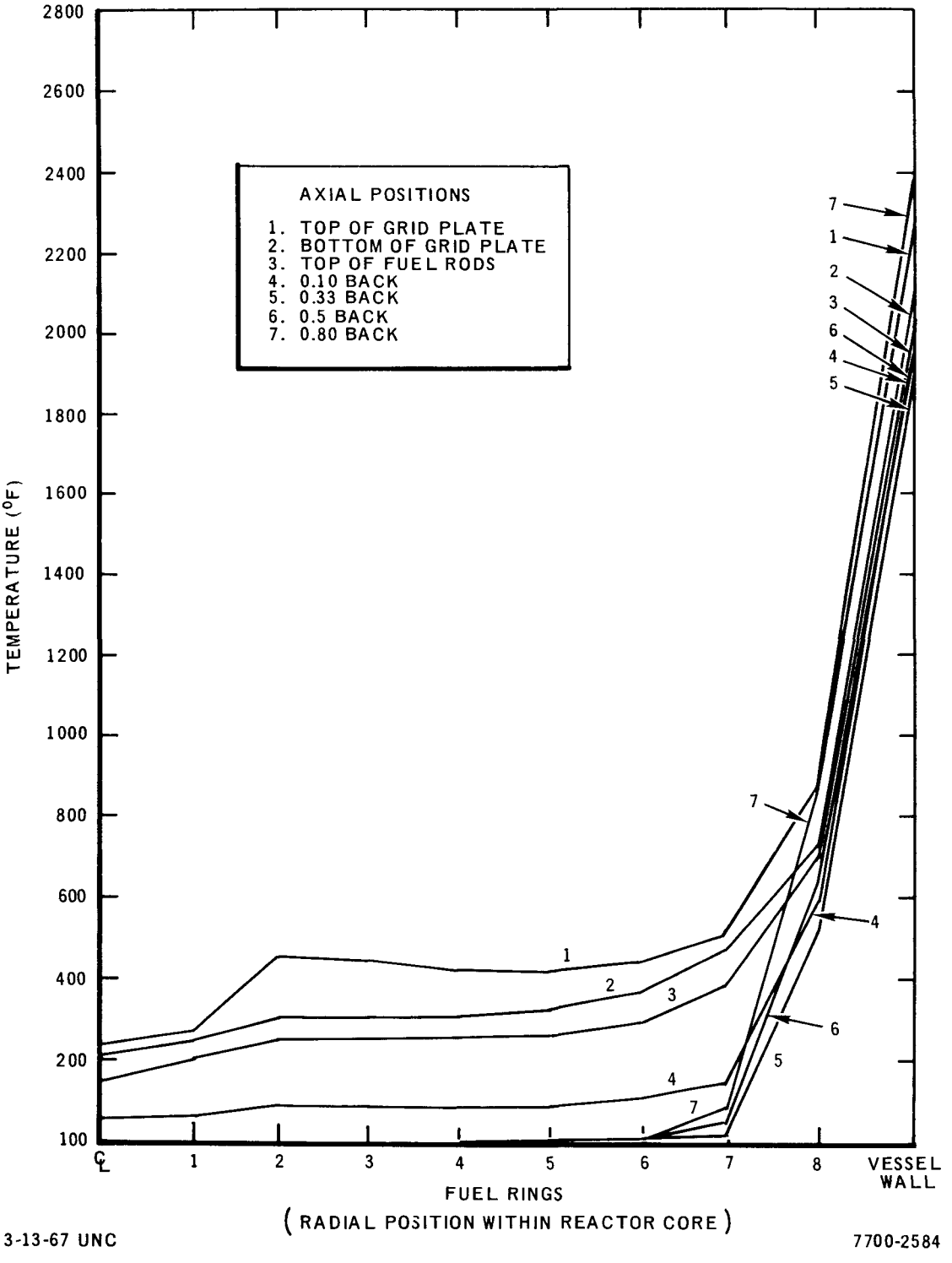

Figure 10. Radial Temperature Profiles of SNAP-8 Reactor (30° Angle-of-Attack, at Time and Altitude of Peak Heating)

central portion of the vessel. Figure B-4 shows the extent of increased heat loading on the lower regions of the vessel wall relative to that on the upper portion of the reactor.

3. 70° Angle-of-Attack Case

Initial ablation takes place at the base of the NaK outlet pipe (Node 41) at 1900 sec, 226,000 ft altitude. See Figure 11 for the temperature vs time traces for various portions of the reactor during reentry. The top head portion of the reactor starts to ablate at Node 106 at 1920 sec, 218,000 ft altitude. At this time and altitude, the unmelted upper portion of the top head (Nodes 101 to 105) will be dispersed from the reactor system. The vertical section of the top head (Nodes 106-108) continues to ablate until Node 219 reaches its melting temperature at 1975 sec, ~188,000 ft altitude. During the next 25 sec of trajectory time, both the upper and lower (Node 359) portions of the reactor's vessel ablate and are dispersed. As seen in Figure 11, the central region of the vessel wall is at a lower temperature due to less aerodynamic heat-loading to that portion of the reactor vessel. The vessel wall has completely dispersed by 2000 sec and an altitude of 194,600 ft. At this time and altitude the core bundle, including grid plates, is completely free of the neutron shadow shield and exposed to direct aerodynamic heating.

The radial temperature profiles for the 70° angle-of-attack reentry case are given in Figure 12. These temperature profiles are quite similar to those of the 30° angle-of-attack case, with the exception that the vessel wall generally attains melting temperature. As in the 30° case, the lower portions of the vessel wall are at a higher temperature than the central regions at the time and altitude of peak aerodynamic heating.

From Figures 7, 9, and 11, it can be seen that the angle-of-attack has considerable effect on the time of upper head melt-through. The reactor's top head was said to be breached when either Node 104 or 106 (whichever was hotter) reached a temperature of 2800°F. Figure 9 shows the α = 30° case taking a longer time for melt-through of the upper head than either the α = 0° or α = 70° cases. This can be explained by considering Table 3 and Figures 5 and 13. Figure 13 shows the time to achieve melt-through of the reactor's top head as a function of angle of attack.

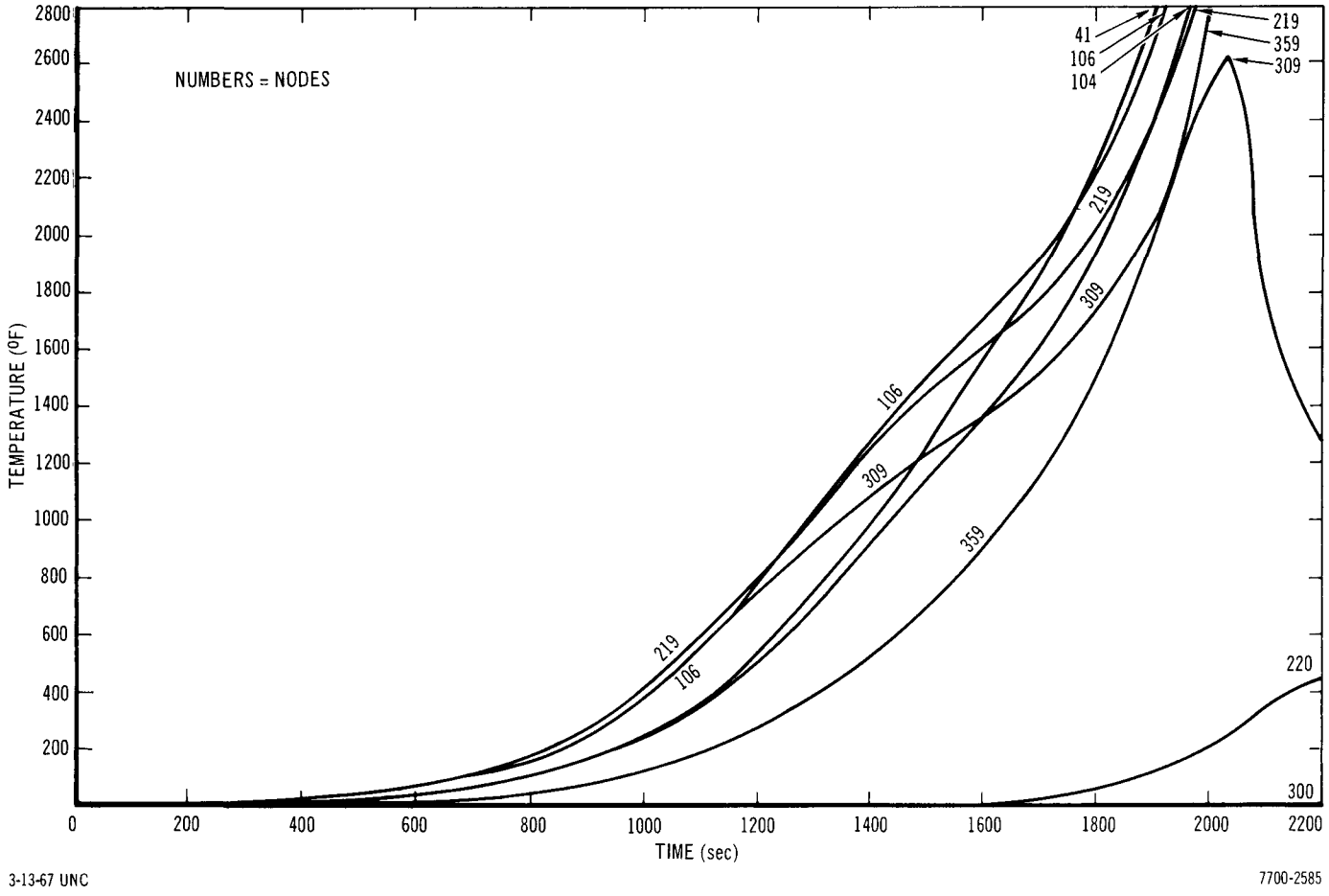

Figure 11. Temperatures of Representative Portions of SNAP-8 Reactor (70° Angle-of-Attack)

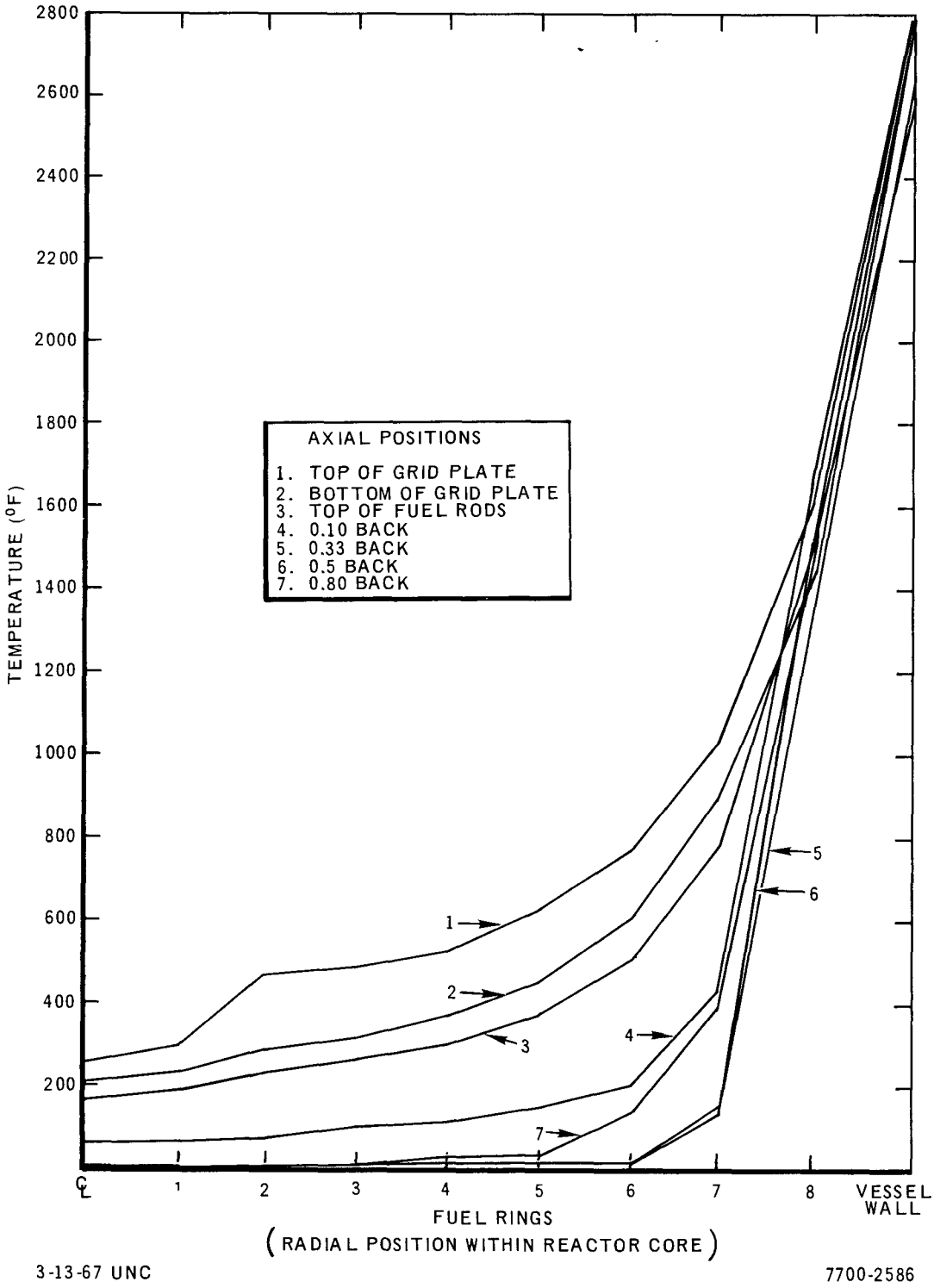

Figure 12. Radial Temperature Profiles of SNAP-8 Reactor (70° Angle-of-Attack, at Time and Altitude of Peak Heating

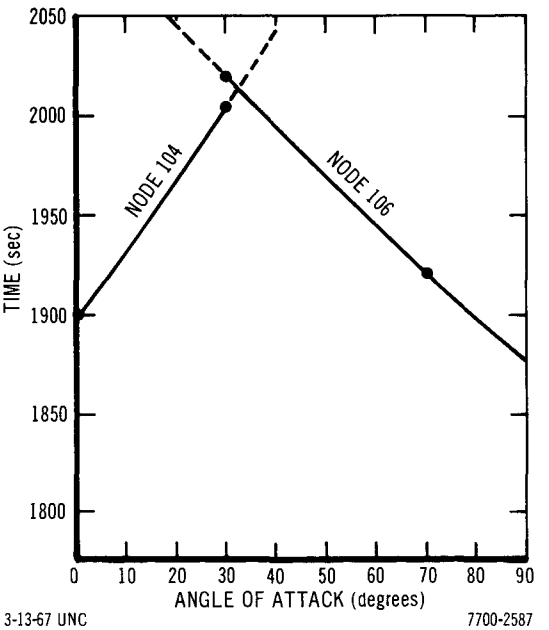

Figure 13. Time to Achieve Melt-Through of Reactor Top Head vs Angle-of-Attack

Node 104 is so situated that the aerodynamic heating is greatest there when system orientation is head-on, and the heating falls off as $\alpha \longrightarrow 30^{\circ}$. On the other hand, Node 106 is on the side, so that it receives its greatest heating during side-on reentry; and the heating falls off as $\alpha \longrightarrow 0^{\circ}$. As a result, during reentry, Node 104 achieves melt-through first for $\alpha = 0^{\circ}$ and 30°, while Node 106 melts through first when $\alpha = 70^{\circ}$. By extrapolating the results given in Figure 13, it can be seen that Nodes 104 and 106 would ablate simultaneously for an angle-of-attack of $\sim 33^{\circ}$.

B. CASE WITH REACTOR DETACHED FROM THE NEUTRON SHADOW SHIELD AND RANDOM TUMBLING INTO THE EARTH'S ATMOSPHERE

A second mode of reentry was considered during which the reactor was assumed to be released from the neutron shadow shield at 400,000 ft, then random-tumbling into the earth's atmosphere. It was hoped that this mode of reentry would enhance ablation and dispersal of reactor components at high altitudes.

A RESTORE Code calculation was made to determine the reference trajectory and heating rates of the SNAP-8 reactor under the second mode of reentry. The results of this calculation are shown as the dashed traces in Figures 3 and 4, where they are compared to the same parameters of the reactor-shield system during the first mode of reentry. In Figure 3 it can be seen that at any given time prior to peak heating the random tumbling reactor has reached a lower altitude and is subjected to a greater q_{ref} than the reactor-shield system during the first mode of reentry. From this it might be assumed that the second mode of reentry would be more beneficial to reactor disintegration than the first mode of reentry. However, when the "effective" aerodynamic heat loading to any given location on the reactor during the two modes of reentry is compared as a function of altitude, it can be seen that the system receives far less heat input under the second mode of reentry. The reference heat rate, q_{ref}, is less, as a function of altitude, during the second mode of reentry, as shown in Figure 4. In addition, the aerodynamic heat-loading correction factor to account for mode of reentry is less for the random tumbling case than for the rotating reactor-shield system, as discussed in Section V. Therefore, the local heat input rates to the rotating reactor-shield system are: $0.36\,(q_{\text{local stag line}})$; where the $q_{\text{local stag line}}$ is given by Equation 2; and the q_{ref}, which is given by the solid trace in Figure 4. Similarly, the local heat input rates to the random-tumbling reactor are: $0.28\,(q_{\text{local stag line}})$, where the $q_{\text{local stag line}}$ is given by Equation 2; and the q_{ref}, which is given by the dashed trace in Figure 4.

From this it may be concluded that the random tumbling mode of reentry does not enhance reactor disintegration, and that the reactor has a higher probability of ablation when attached to the neutron shadow shield during reentry. For this reason, a calculation was not made using the TAP-3 analytical model of the SNAP-8 reactor.

VII. CONCLUSIONS

From the results of this analysis, it is concluded that the SNAP-8 reactor vessel will not ablate to a sufficient extent, for probable modes of reentry, to release the fuel elements at altitudes necessary to obtain complete fuel ablation.

An earlier study[4] showed that the SNAP-10A, zirconium-uranium-hydride fuel elements would have to be released from the reactor core by ~250,000 ft in order to fully ablate upon reentry. Based upon this work, it has been calculated that the SNAP-8 fuel element, composed of the same fuel material but of smaller dimension, must be released by ~210,000 ft to fully ablate.

By comparing the amount of heat radiated per unit area from the stainless steel vessel at melting temperature with the amount of heat available for the given trajectory, it was found that the vessel could reach melting temperature at an altitude of 292,000 ft, neglecting heat capacity effects. Taking the melting temperature of SS 316 as 2600°F and its thermal emissivity as 0.7, the reactor vessel will radiate 29.2 Btu/ft^2-sec to space. This quantity of heat is available during the trajectory after the reactor has reached an altitude of 292,000 ft. Taking the melting temperature of SS 316 as 2800°F, the reactor vessel will radiate 37.4 Btu/ft^2 sec. The trajectory reference heat rate equals this quantity at 283,000 ft.

The detailed thermal study, described herein, was undertaken to determine the actual thermal response of the vessel to the reentry environment. This study showed that initial ablation of the reactor's top head does not occur until altitudes of 234,000 and 209,000 ft for the 0° and 30° angle-of-attack cases, respectively, which were investigated under the first mode of reentry. During both of these cases, the reactor vessel was intact and at temperatures well below melting at time and altitude of peak heating. The altitude of peak heating, 151,000 ft, is far below the minimum required release altitude to obtain fuel element ablation.

Even for the highly improbable 70° angle-of-attack reentry case, the vessel wall did not fully ablate until an altitude of 194,600 ft had been reached. This altitude is also below the minimum fuel element release altitude.

It is evident that some vessel ablation will occur during reentry, particularly in the NaK outlet pipe and top head portion of the reactor. Even though this initial ablation occurs at relatively high altitudes, the vessel wall will not ablate until altitudes well below the minimum fuel element release altitude. For this reason, it is further concluded that portions of the SNAP-8 fuel elements will survive reentry.

REFERENCES

1. R. W. Detra and H. Hidalgo, "Generalized Heat Transfer Formulas and Graphs for Nose Cone Reentry Into the Atmosphere," American Rocket Society Journal (March 1961)

2. M. Jakob, Heat Transfer, Vol. I, Wiley and Sons, New York (1949)

3. R. D. Elliott, "Aerospace Safety Reentry and Experimental Program, SNAP-2 and 10A," NAA-SR-8303 (September 1963)

4. A. W. Barsell, L. D. Montgomery, and J. E. Arnold, "Thermal Behavior of SNAP Reactor Fuel Elements During Atmospheric Reentry," NAA-SR-11502 (March 1966)

5. L. Lees, "Laminar Heat Transfer Over Blunt-Noses Bodies at Hypersonic Flight Speeds," Jet Propulsion, Vol. 26, No. 4 (April 1956)

6. L. Bogdan, "High Temperature Heat Transfer Gages (High Temperature Thin-Film Resistance Thermometers for Heat Transfer Measurements)," I. E. E. E. Paper No. CP 63-381 (1963)

7. G. T. Skinner, "Calibration of Thin-Film Gage Backing Materials," ARS Journal, Vol. 31, No. 5 (May 1961)

8. R. J. Vidal, "Transient Surface Temperature Measurements," Cornell Aeronautical Laboratory, Inc., CAL Report No. 114 (March 1962)

9. J. E. Arnold and L. D. Montgomery, "SNAP Reactor Ablation-Disintegration Experiment (RADE) in a Hyperthermal Wind Tunnel," NAA-SR-12383 (to be published)

10. D. K. Nelson, "SNAP 8 Configuration Reentry Hypersonic Heating Rates Derived From a Shock Tunnel Test," NAA-SR-12383 (to be published)

APPENDIX A
REACTOR ABLATION DISINTEGRATION EXPERIMENT

A. INTRODUCTION

The Reactor Ablation Disintegration Experiment (RADE) was conducted to measure the aerodynamic heat flux to the complicated geometry of SNAP reactors and to demonstrate the capability and accuracy of the analytical techniques used in the reactor disintegration analysis.*

Half-scale models of the SNAP-10A (RADE-A) and SNAP-8 (RADE-B) nuclear reactor configurations were tested in the NASA Ames hyperthermal wind tunnel under simulated atmospheric reentry conditions. Surface heat flux measurements were made with calorimeter models (Figure A-1), employing asymptotic calorimeter heat sensors. The experimental RADE models (Figures A-3 through A-6) were ablated at both 0° and 30° angles of attack in the flow stream. The temperature response of the models to the aerodynamic heating of the jet stream was obtained throughout each test run from thermocouples strategically mounted in the models.

Throughout each ablation test, event motion picture film coverage (24 frames per second) and high-speed motion picture film coverage (128 frames per second) were obtained which provided a detailed visual description of the sequence of events during reactor ablation disintegration. These events clearly defined the meltdown and mode of disintegration of the reactor components under simulated reentry conditions.

B. TEST DESCRIPTION

1. Facility Description

The RADE test was performed in the hyperthermal wind tunnel of the Gasdynamics Branch Facility at NASA Ames Research Center, Moffett Field, Calif. This facility is capable of producing nominal Mach 5 gas flow at extremely high temperatures. The flow is produced by injecting air into the plenum of a Linde arc-heater, used in conjunction with a 10-Mw power supply. The arc-heated air is expanded through a conical, supersonic nozzle to a 24-in. diameter exit plane. A simplified schematic diagram of the test facility is shown in Figure A-2.

*This work has been reported in greater detail in Reference 9

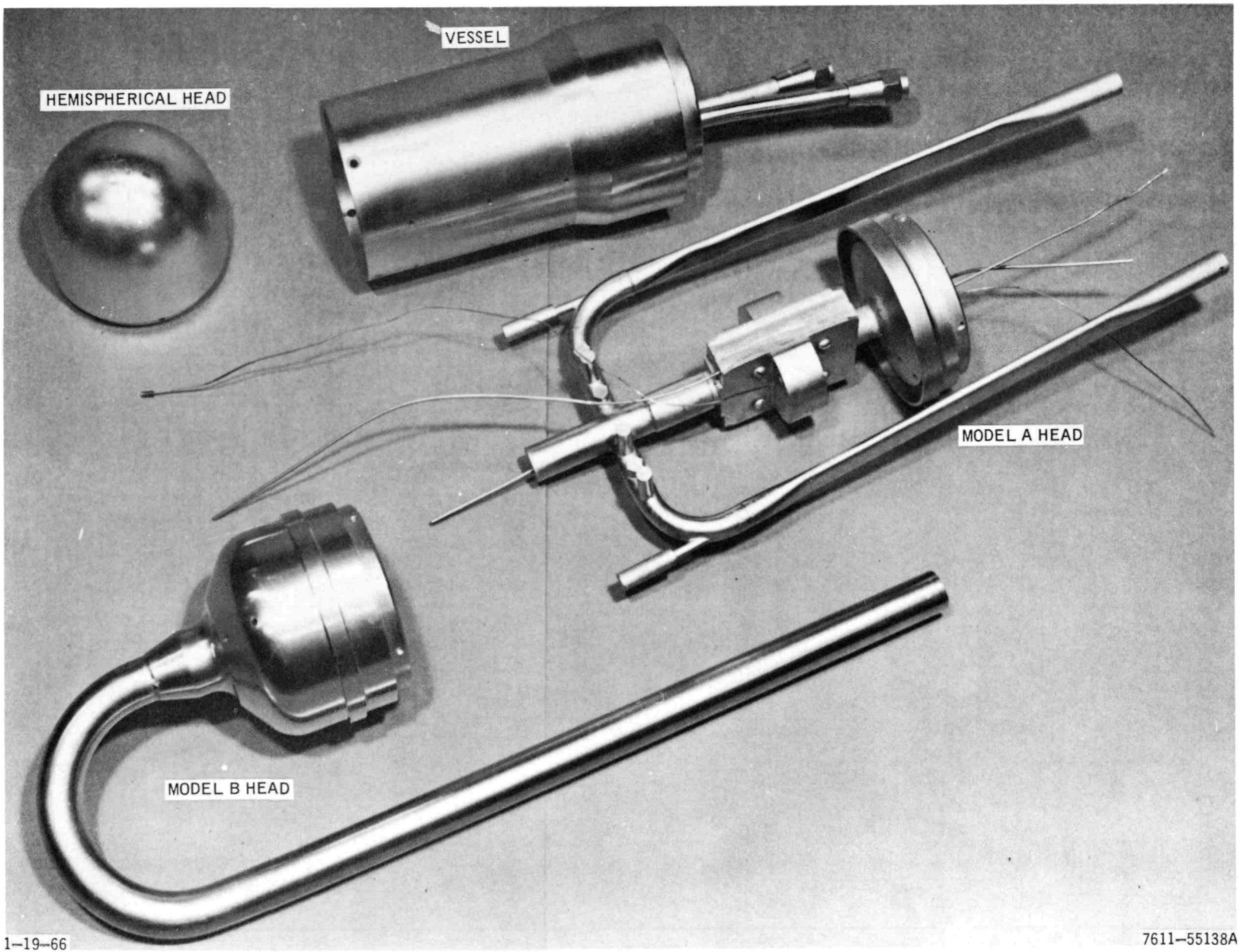

Figure A-1. RADE Calorimeter Model and Head Configurations

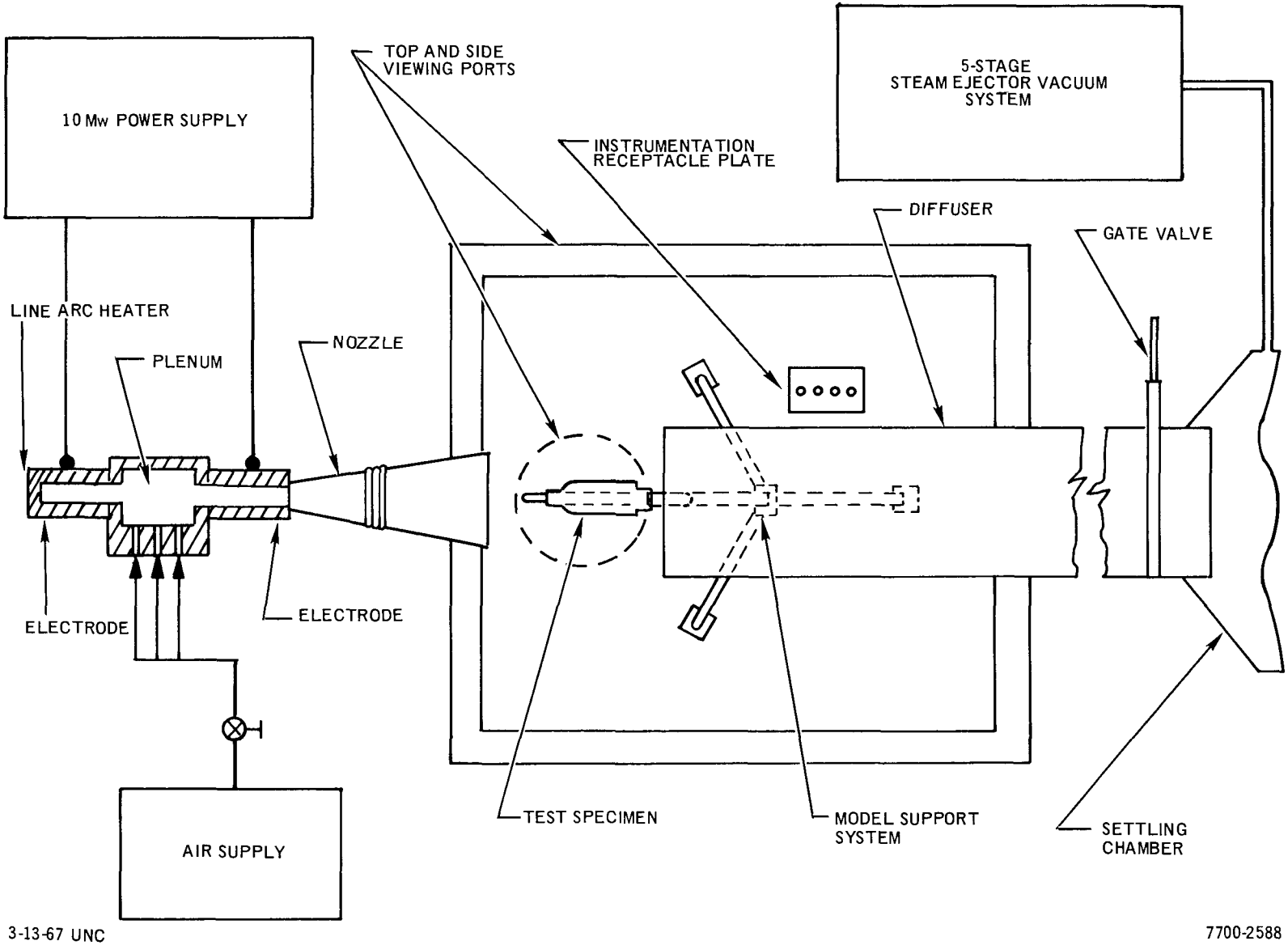

Figure A-2. Simplified Schematic Diagram of NASA-Ames Hyperthermal Wind Tunnel

2. Model Description and Instrumentation

a. Reactor Ablation Models

The RADE ablation models were half-scale replicas of SNAP-10A and 8 flight reactor configurations, restricted basically to the external geometry (other components were scaled as required to insure duplication of the thermal characteristics). The ablation model complement included two SNAP-10A and two SNAP-8 configurations, one each to be tested at 0° and 30° angles of attack.

The RADE-A model consisted of a NaK pipe and simulated thermoelectric pump assembly welded to the head of a cylindrical vessel enclosing the reactor core components. Three NaK tubes protruded forward from the transverse section of the NaK pipe; the central tube is a fill tube and the outer tubes are overflow tubes. Six simulated thermoelectric switches extended through the transverse pipe normal to the NaK fill and overflow tubes. The pump assembly, positioned between the vessel head and transverse NaK pipe, consisted of a pump housing containing the central NaK outlet pipe, one pair of Alnico magnets, two pump fixtures, and four plane radiator surfaces (pump fins). The exterior dimensions of the NaK piping were half-scale with full-size wall thickness as was the case for the pump fins. The pump itself was half-scale and, although void areas were duplicated by extensive simplification of parts, the general assembly concept was maintained. The pump and NaK pipe assemblies were secured to the vessel head at its center by two pump support brackets and four support legs. The NaK downcomer pipes were secured to the outer periphery of the vessel head by two spacer blocks.

The cylindrical vessel shell of the models housed 2 grid plates, 6 internal reflectors, and 37 fuel elements. The vessel shell was one-half the scale of a SNAP-10A flight reactor with full-scale wall thickness. The upper and lower grid plates positioned the fuel elements and internal reflectors inside the vessel. The upper grid plate (located under the top head) was half-scale with full-scale thickness, and its installation conformed to the SNAP-10A configuration. The lower grid plate was the half-scale concept of the SNAP-8 configuration with the half-scale SNAP-10A fuel rod hole pattern. The internal reflectors were half-scale to the SNAP-10A internal reflectors. The fuel elements were

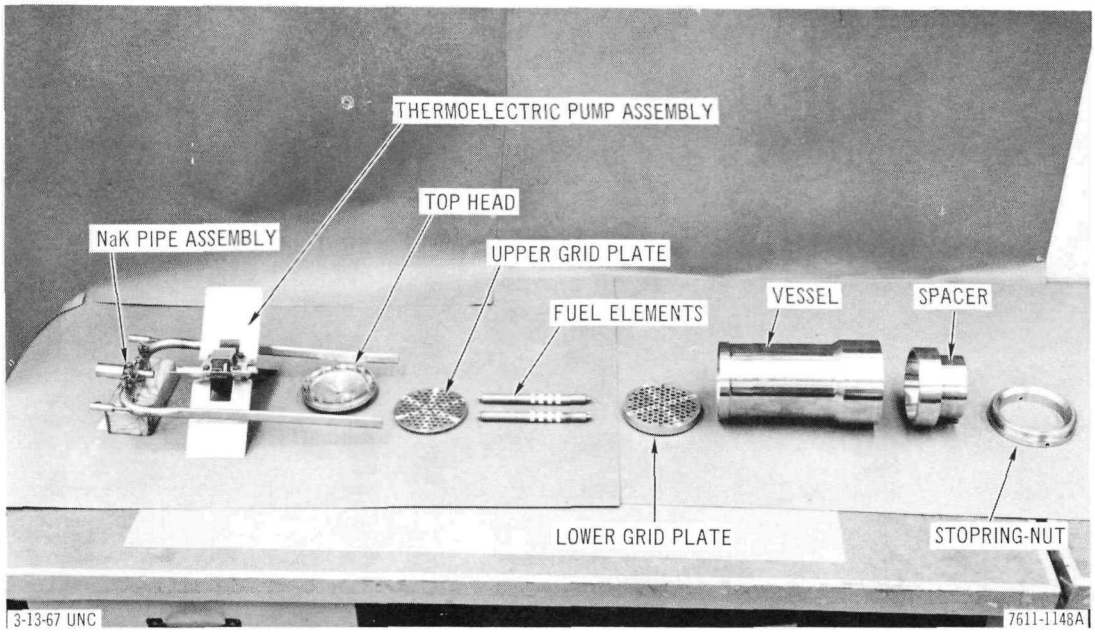

Figure A-3. Disassembled RADE-A Model
Showing Major Components

of the full-scale SNAP-8 configuration (0.56-in. diameter) reduced to a length of 6.3 in. With the core assembly in place, a stopring-nut assembly was threaded into the bottom of the reactor vessel to secure the components and to serve as an attachment fixture to the support equipment. The RADE-A model major components are shown in Figure A-3 and the assembled model (not welded) is shown in Figure A-4.

The RADE-B model consisted of a U-shaped NaK pipe, a hemispherical-shaped vessel head, and a cylindrical reactor vessel, all half-scale to the SNAP-8 configuration in external dimensions with full-scale wall thicknesses. The NaK pipe was welded to the head, which in turn was welded to the reactor vessel. The core components were identical with those of the RADE-A model except for the upper grid plate, which was half-scale to the upper grid plate of the SNAP-8 configuration with full-scale thickness. The RADE-B model major components are shown in Figure A-5, and Figure A-6 shows the assembled model.

The individual model components were fabricated from like materials of their actual counterparts. This, for the most part, was Type 316 stainless

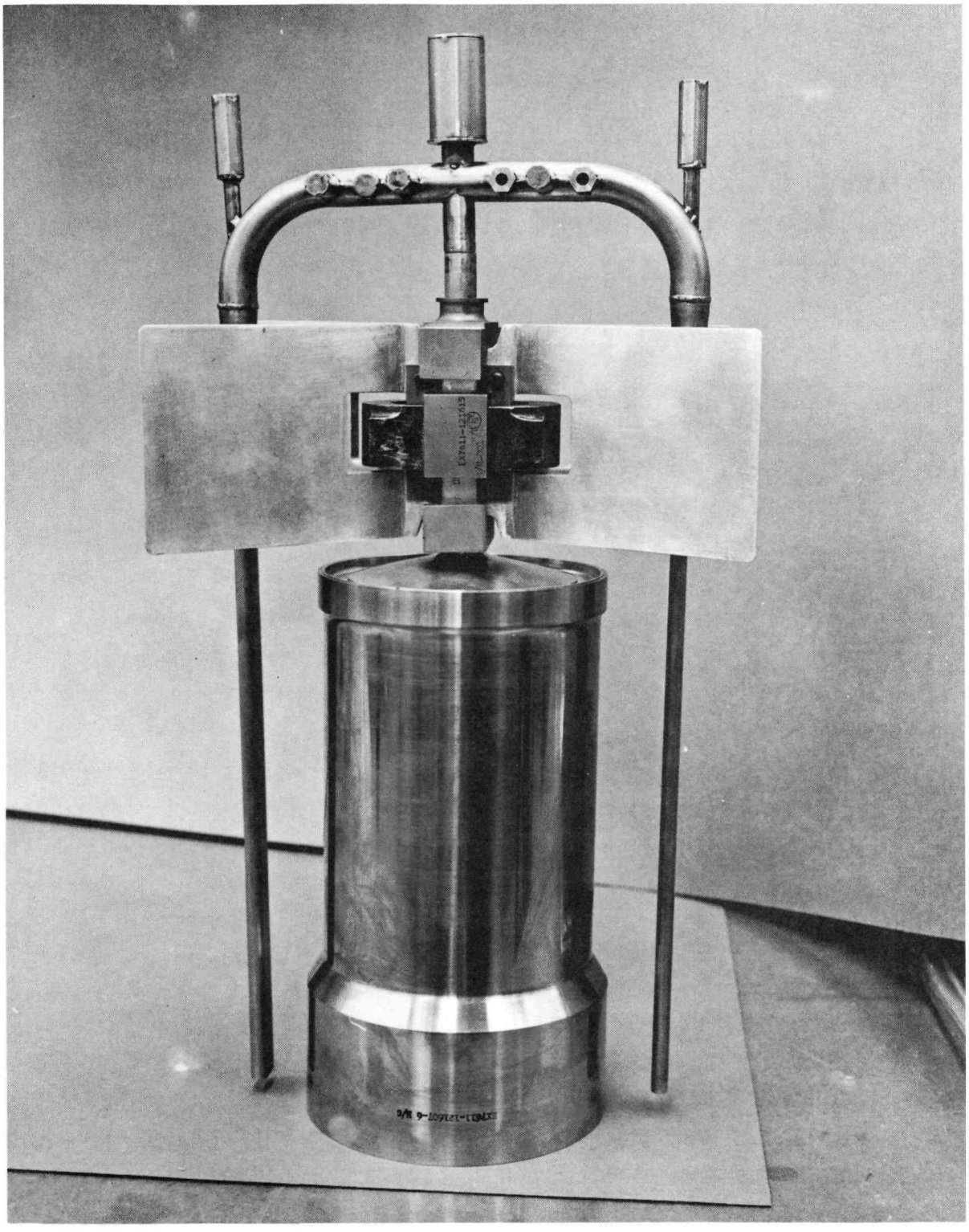

6-28-65 UNC 7611-1147

Figure A-4. RADE-A Ablation Model

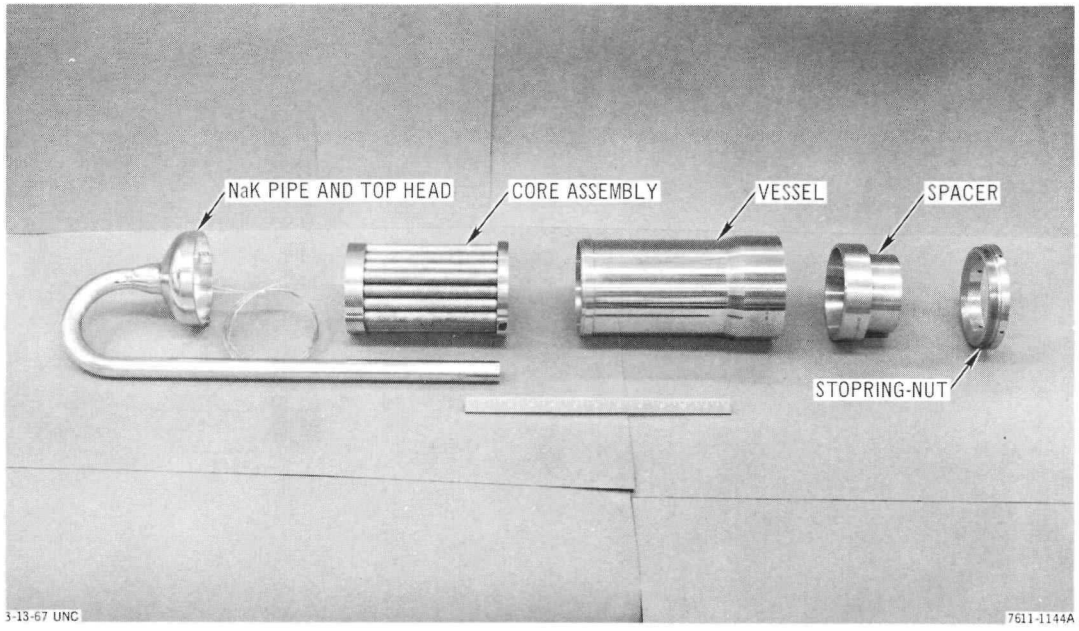

Figure A-5. Disassembled RADE-B Model Showing Major Components

steel, except for the fuel elements, internal reflectors, and RADE-A pump components. The fuel rods were zirconium-hydride (H/Zr = 1.75), containing no uranium, and clad with Hastelloy-N which was internally coated with a non-classified ceramic. The internal reflectors were made of a commercial grade Monel in place of beryllium, since it closely duplicates the thermal properties of the actual reflector material and is not toxic. These substitutions of core materials eliminated the health safety hazard associated with nuclear and toxic materials. The pump radiator surfaces (pump fins) were aluminum, the magnets were Alnico, and the pump fittings were a titanium-aluminum-vanadium alloy.

b. Instrumentation

The RADE-A and RADE-B models were instrumented with 0.02-in. OD chromel-alumel thermocouples located in the NaK pipe, head, grid plates, fuel rods, radiators, and vessel wall. The 0.02-in. OD thermocouples were used in place of the preferred 0.04-in. OD to minimize the effect of the introduced condition paths of the leads and sheathing. The thermocouples were welded

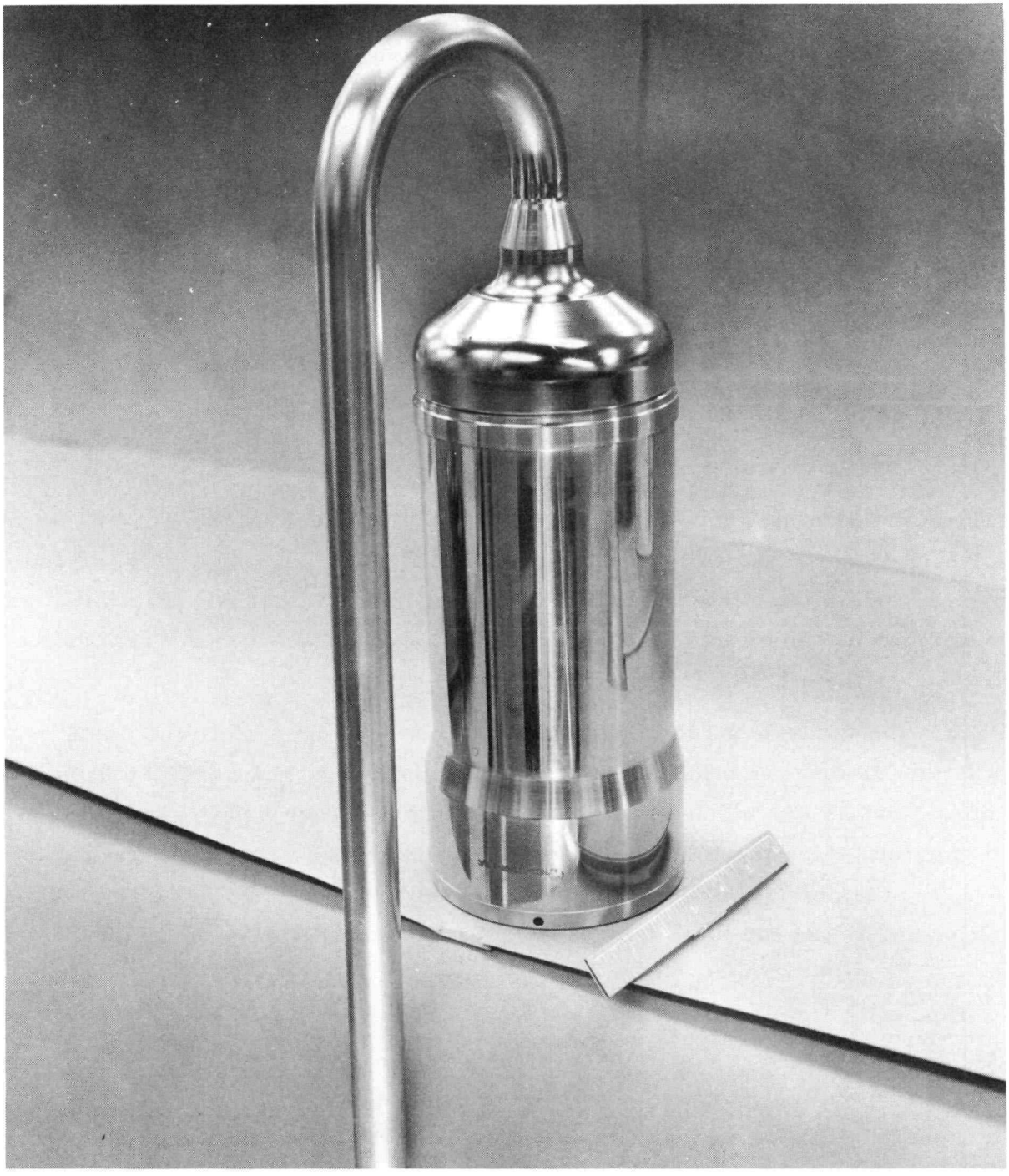

4-9-65 UNC 7611-1145

Figure A-6. RADE-B Ablation Model

into the various surfaces, with the stainless steel sheathing routed internally through the vessel core to the base of the model, where 10 ft of flexible lead per thermocouple was spliced to the sheaths. The flexible lead bundle was braided to prevent possible capacitive pickup, and connected to two electrical plugs. A total of 30 thermocouples were mounted in the RADE-A model, and 25 in the RADE-B model.

Temperature sensitive paints were applied to the grid plates, fuel rods, and internal reflectors of both RADE-A and RADE-B models to supplement the thermocouple instrumentation. Strips of different temperature level points were used to cover a range of maximum anticipated temperatures since the exact mode of disintegration was difficult to predict.

C. TEST RESULTS AND ANALYSIS

1. Calorimeter Tests

Three calorimeter models were used to obtain heat flux measurements over the RADE-A and B experimental models under test conditions. Two of the calorimeter models duplicated the RADE-A and B configurations. The third calorimeter model consisted of a hemispherical head attached to the reactor vessel calorimeter model.

From the measured readings of the heat sensors located in the dome head model, local-to-stagnation point heating ratios (q_l/q_{stag}) were calculated. The resulting ratios are plotted in Figure A-7 as a function of angle from the stagnation point. Also plotted in the figure is a theoretical curve for the ratio q_l/q_{stag} obtained from the work of Lees (Reference 5). The excellent agreement of the measured ratio with that of theory substantiates the validity of the measured data at the stagnation point for use as a standard value of reference heat flux.

The heat sensors in the RADE-A and B calorimeter models gave similar, local-to-stagnation point heating ratios (q_l/q_{stag}), for various positions on the respective ablation models. These values were used to correlate the analytical and experimental results.

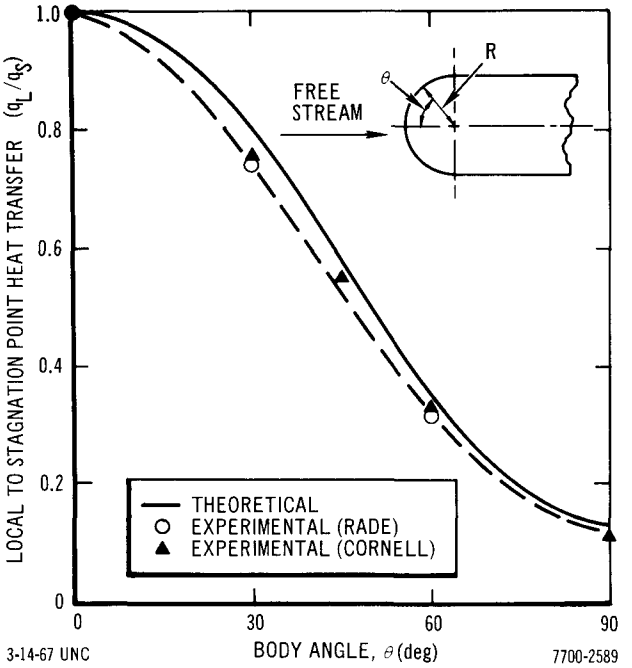

Figure A-7. Heat Transfer Distribution Around Hemispherical (Dome) Heat Calorimeter

2. Ablation Tests – Results and Analysis

a. Analytical Model Description

A Thermal Analyzer Program (TAP) analog was developed to represent a 180° portion of each RADE experimental model configuration. A detailed description of this computer code is given in Section IV of this report. These models were used in correlating the RADE ablation data to analytical methods. The thermophysical properties used in making the various analytical calculations are the same as given in Section III.

b. Correlation of Analytical and Experimental Results

The experimental temperature results for the four ablation cases were converted to temperature-vs-time traces. Correlation of the analytical cases, simulating the four test conditions, to the corresponding experimental results was completed using the TAP models and the heat input rates from the calorimeter measurements.

Representative temperature-vs-time traces for various positions on the RADE-A and RADE-B, 0° angle-of-attack cases illustrating the overall extent

of correlation between experimental and analytical results are given in Figures A-8 through A-15.

The temperature-vs-time traces of the various external thermocouples on the RADE test models become erratic after short periods of time. This may be attributed to either the change in local heat input due to dispersal of reactor components or to molten metal hitting the thermocouple locations. RADE-A, 0° thermocouples 20 and 21 (see Figures A-8 and A-9, respectively) are smooth in shape until they ceased to function after approximately 2 sec. At this time, the NaK cross-pipe began to ablate and break away. The erratic behavior of thermocouples 16 and 13 (see Figures A-10 and A-11, respectively), during the same test case, was caused by molten metal hitting these thermocouple locations.

The NaK outlet pipe began to ablate away at approximately 5 sec during the RADE-B, 0° angle-of-attack test case. Because of this, thermocouples 25 (see Figure A-12) and 22 (see Figure A-13) ceased to function at 6 and 4.5 sec, respectively. During the same test case, thermocouple 19 (see Figure A-14) became erratic and was lost at approximately 22.5 sec. The sharp increase in

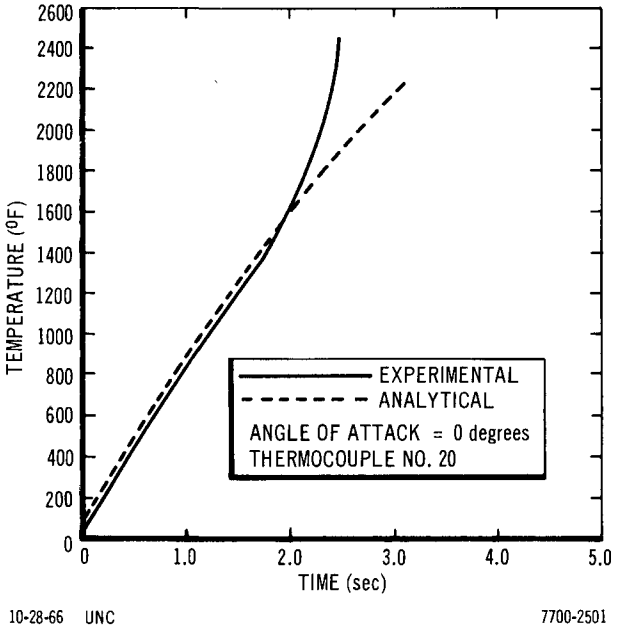

Figure A-8. RADE-A Temperature vs Time Traces (Top of NaK Cross Pipe)

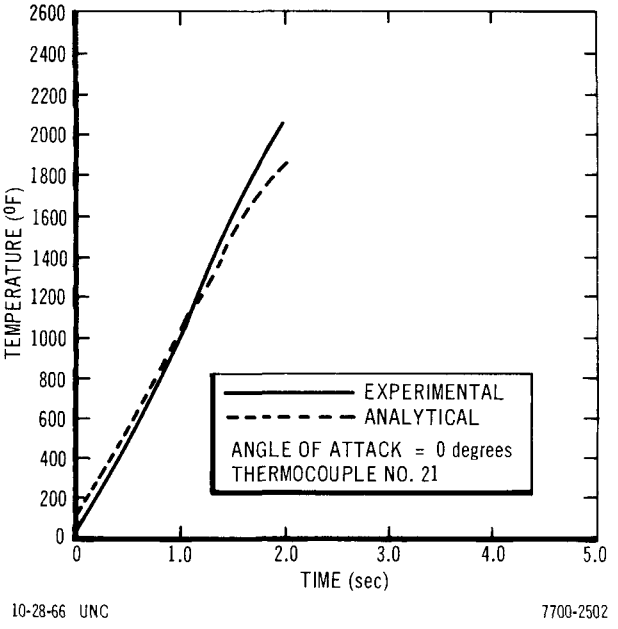

Figure A-9. RADE-A Temperature vs Time Traces (Top of Thermal Switch on NaK Cross Pipe)

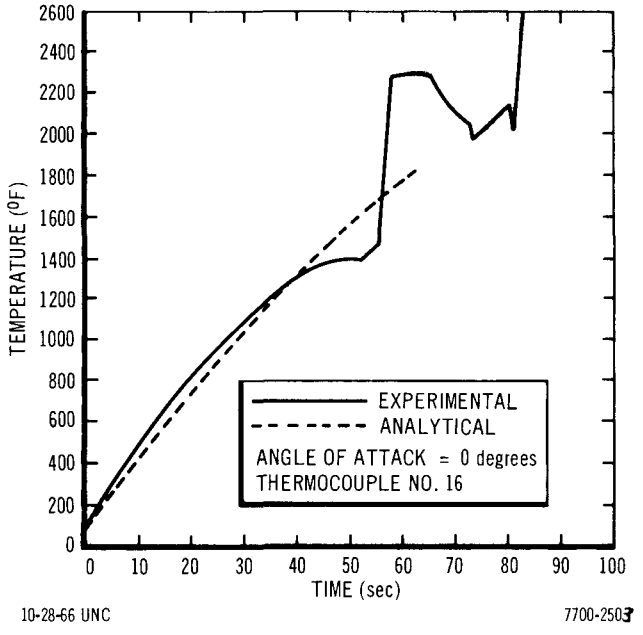

Figure 10. RADE-A Temperature vs Time Traces (Trailing Edge of Cooling Fin)

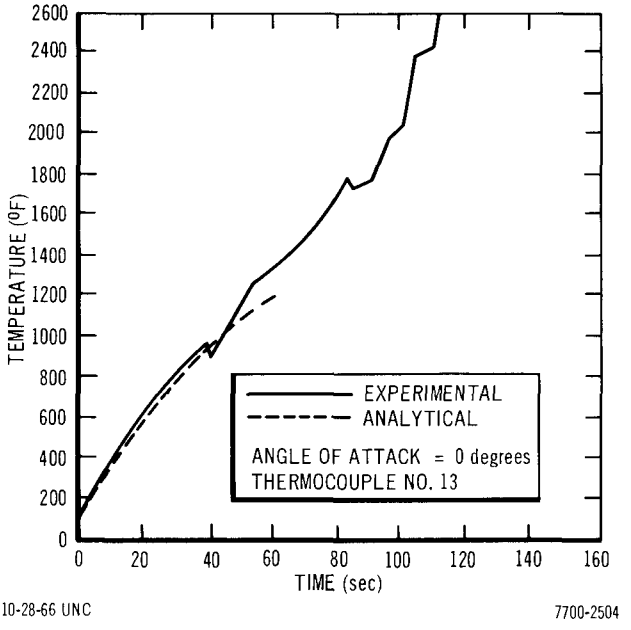

Figure A-11. RADE-A Temperature vs Time Traces (Lip of Top Head)

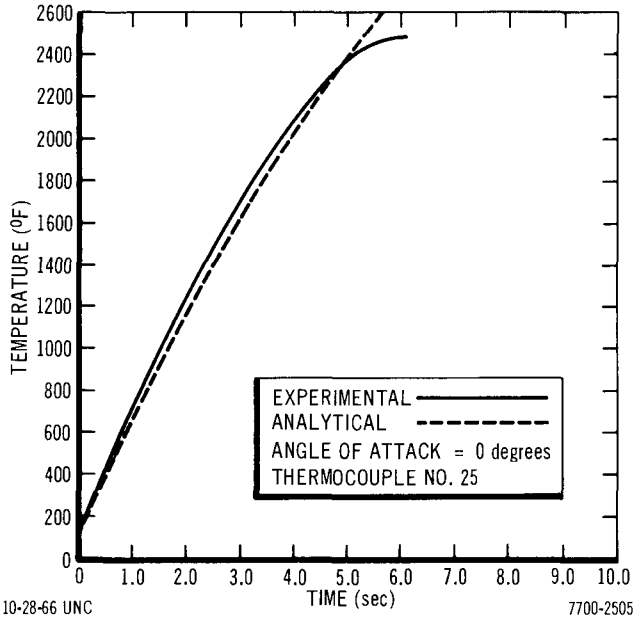

Figure A-12. RADE-B Temperature vs Time Traces (Top of NaK Outlet Pipe)

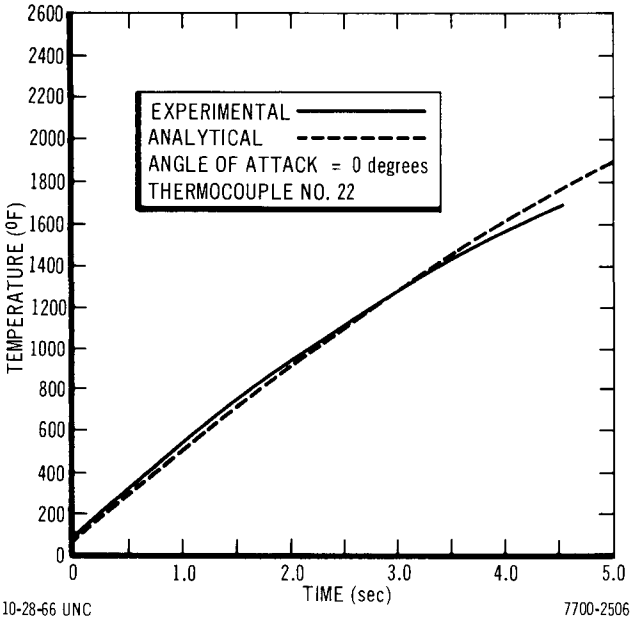

Figure 13. RADE-B Temperature vs Time Traces (45° From Top of NaK Outlet Pipe)

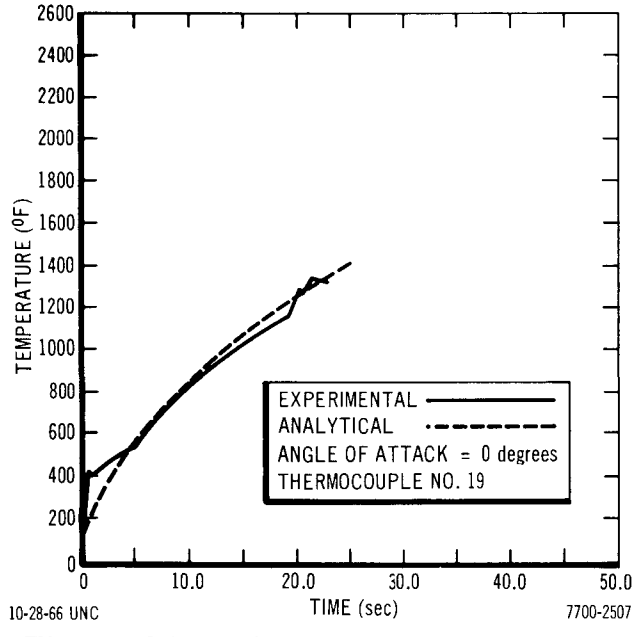

Figure 14. RADE-B Temperature vs Time Traces (Top Head, Not Behind NaK Outlet Pipe)

temperature experienced by thermocouple 20 (see Figure A-15) during the RADE-B, 0° case was caused by molten metal from the dispersing NaK outlet pipe hitting the thermocouple.

The analytical results obtained from the analogs compare reasonably well with those of the four experimental cases. Better correlation between the analytical and experimental results was obtained for the two RADE-B ablation runs than for the two RADE-A tests. This may be attributed to the simplicity of the external configuration of the RADE-B reactor model.

D. SUMMARY AND CONCLUSIONS

In summary, the RADE test series was highly successful in satisfying the primary test objectives. Aerodynamic heat flux measurements, obtained with the calorimeter model, provided to a SNAP reactor experimental local heat rates that, previously, were based on theory. These measurements were utilized as initial condition input to analogs of the models, resulting in good correlation of the analytical calculations with the experimental temperature response of the models. Therefore, experimental support of the analytical capability to accurately predict the preablation temperature response of SNAP reactors reentering the earth's atmosphere has been achieved.

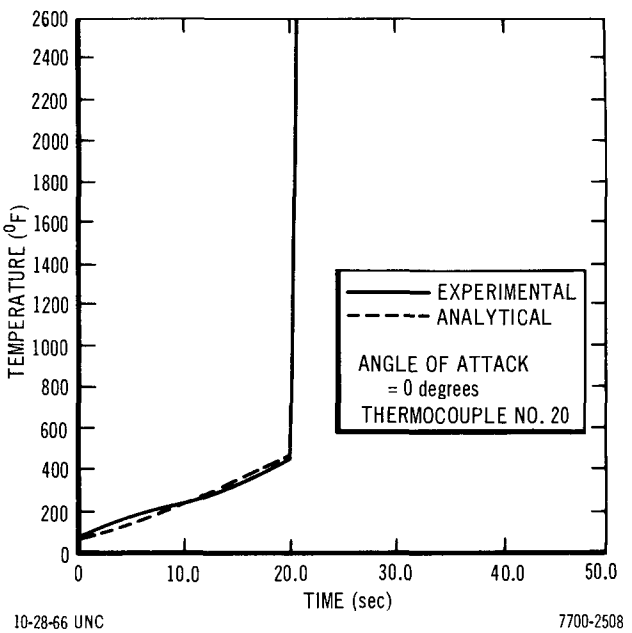

Figure A-15. RADE-B Temperature vs Time Traces (Top Head, Behind NaK Outlet Pipe)

APPENDIX B
CORNELL AEROHEATING EXPERIMENT

A. INTRODUCTION

Reentry aerodynamic heating distributions for the SNAP-8 configuration were obtained based on hypersonic shock tunnel experiments.* The heat transfer correlations were determined as a function of angle of attack from 0 to 70°. The local aerodynamic heating factors for the 0, 30, and 70° angle-of-attack cases obtained in this experiment formed the basis of the heating distributions used in the three analytical calculations considered under the first mode of reentry.

B. TEST OBJECTIVES AND REQUIREMENTS

1. Facility Description

The Cornell Aeronautical Laboratory 48-in. hypersonic shock tunnel was selected for determining the aerodynamic heating distribution on the SNAP-8 configuration. A schematic of the CAL 48-in. hypersonic shock is presented in Figure B-1. The basic shock tunnel components are the shock tube, expansion nozzle, and model support and instrumentation systems. The shock tube is separated into regions of high (driver gas) and low (driven test air) pressure by a set of diaphragms; the pressure and temperature ratios dictate the flow conditions and must be set to give a tailored interface for the driver-to-driven gases. The downstream end of the shock tube is terminated by a convergent-divergent nozzle where the area ratio of the nozzle throat shock tube cross section is small. This has the effect of almost completely reflecting the primary shock wave upstream from the throat, leaving a region of almost stagnant, compressed, and heated air at the end of the low-pressure section of the shock tube. This processed air is then expanded through the nozzle to the desired hypersonic conditions.

2. Model-Description

The aero-heating model design was based on criteria set to satisfy the test objectives. Therefore, the model configuration was selected to be representative of a reactor system at reentry into the upper atmosphere of the earth after a space mission. The model drawing of the SNAP-8 reactor, radiation shield,

*This work has been reported in greater detail in Reference 10.

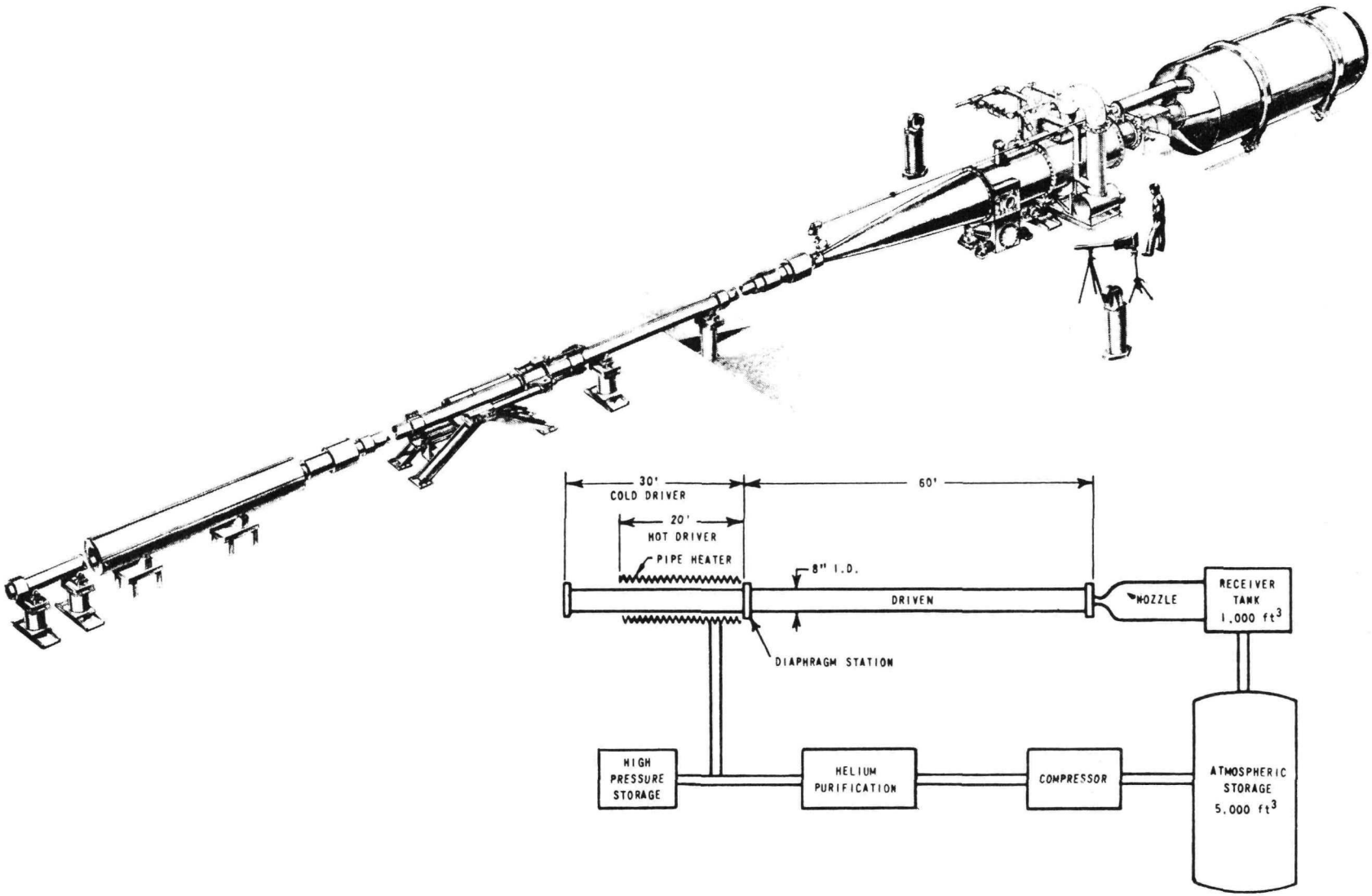

7-11-66

7611-2521

Figure B-1. Basic Components of Cornell Aeronautical Laboratory 48-in. Hypersonic Shock Tunnel

and system piping is presented in Figure B-2. The model tunnel support system was designed so that the model could be oriented at any desired combination of angle-of-attack and roll from 0 through 90 and 360°, respectively. This freedom of positioning allowed the measurement of aerodynamic heat transfer rates where flow perturbation, due to piping over the basic body configuration, ranged from negligible to maximum in degree.

The aero-heating model was scaled to one-fifth of actual system size. This physical size was small enough to be accepted by the CAL 48-in. hypersonic shock tunnel and large enough to house the 44 heat-transfer gages installed on the model. The placement of heat transfer gages on the model was made with a concentration on the reactor vessel section. This resulted in a distribution of 8, 25, and 11 heat-transfer sensors on the piping, reactor vessel, and radiation shield, respectively. Heat transfer gage locations are shown on Figure B-2.

3. Flow Conditions

The flow conditions were based on criteria established to provide heat transfer data in the reentry hypersonic continuum flow regime. To be more specific, the flow must correspond to the environment that would be experienced by a SNAP configuration (Figure B-2) during the early aerodynamic heating phases of continuum flow. These flight conditions are represented by high altitude and velocity well before the maximum heating point in the reentry trajectory is reached. With these criteria in mind, the test condtions were set at a unit Reynolds number of 35,000, corresponding to a simulated altitude of 250,000 ft for a one-fifth scale model and a free-stream Mach number of 18.4 for flow field similitude.

4. Heat Flux Gage

The heat transfer measurements were accomplished by use of the thin-film heat transfer gages described in References 6 and 7. These devices were inserted, or integrally fabricated, into the model at specified locations. During the test interval of just less than 4 msec, each of the sensors measured the temporal variations in local surface temperatures. This limited test time required an extremely fast response and dictates the use of the thin-film heat transfer gage.

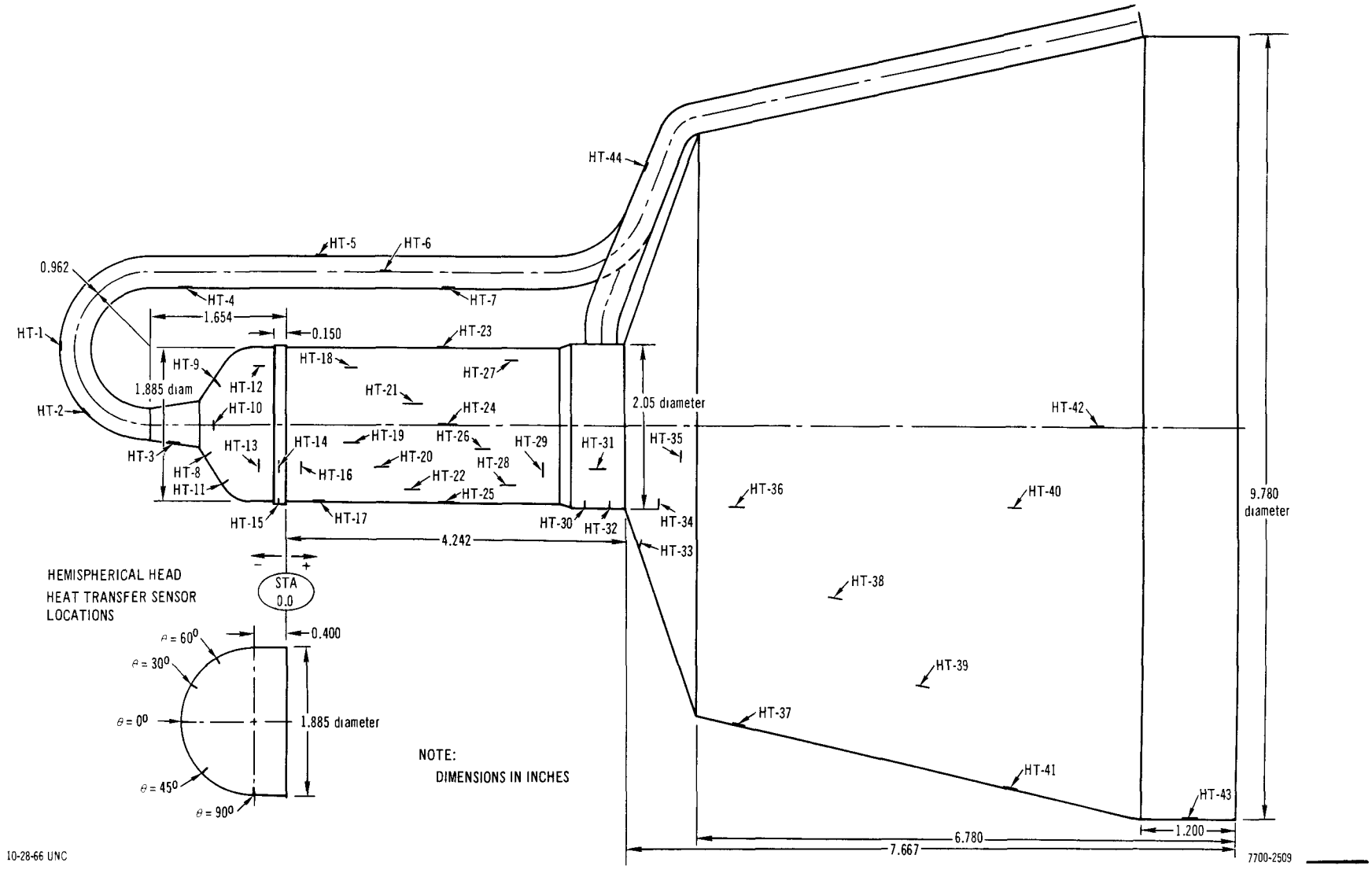

Figure B-2. Aeroheating Test Model Heat Transfer Sensor Locations

C. TEST DATA AND CORRELATIONS

1. Hemispherical Head Calibration Run

Heat-transfer data were acquired at a zero-degree angle-of-attack position, with a hemispherical head on the reactor vessel in place of the dome head and piping. The hemispherical head was equipped with heat transfer sensors at body angles of 0, 30, 45, 60, and 90°. These data were obtained to substantiate the predicted theoretical aerodynamic heat transfer rates based on tunnel air flow conditions and to establish an experimental base line for the series of tests. The ratio of local-to-stagnation heat transfer rates on the hemispherical nose are compared in Figure A-7 to the theoretical distribution developed by Lees (Reference 5).

2. SNAP-8 Configuration Results

Heat-transfer data were acquired from the sensor locations noted on Figure B-2. A series of 12 heat-transfer acquisition runs were made for the SNAP-8 configuration. These test runs were performed in 10° angle-of-attack steps from 0 to 70° with the piping in the shadow of the flow (zero roll), and for piping spatial roll positions of 90 and 180° at 30 and 60° angles-of-attack. All aerodynamic heat-transfer data obtained from the test have been normalized by the calibration hemispherical stagnation point value, and are presented in a schematic distributional form on the reactor vessel and piping. These are given for flow impinging on the model at 0, 30, and 70° in Figures B-3, B-4, and B-5, respectively. These heat-transfer distributions on the SNAP-8 configuration represent overall equilibrium conditions at the selected static orientations to the airflow. The stagnation line local heat distributions shown in Figures B-3, B-4, and B-5 were used in the analytical calculations simulating the SNAP-8 system under the first mode of reentry.

In general, all heat-transfer trends are substantiated by theory. Examples and an explanation of some of the flow phenomena are given in the following paragraphs. The heat transfer on the forward areas of the piping (Sensors 1 and 2 in Figure B-2) exhibit smooth correlations where the shock wave lies closely over the body; however, other portions of the piping show the effects of a changing secondary flow field. This can be seen on the piping segment just above the head (Sensor 3 in Figure B-2), where heat transfer is influenced by

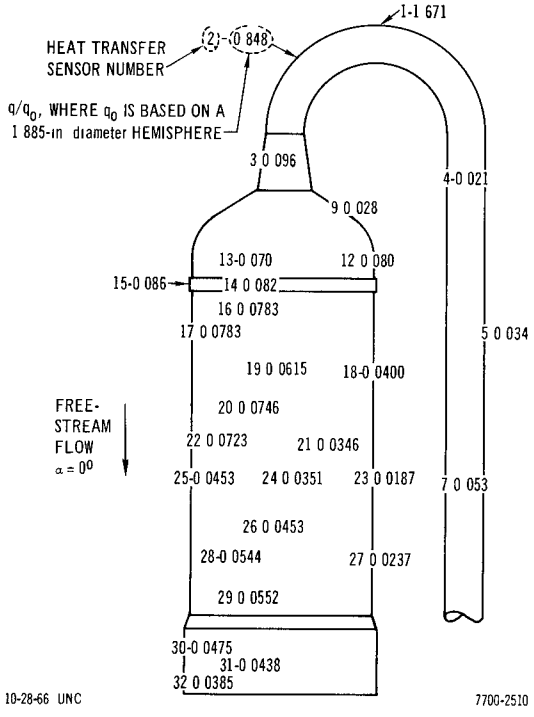

Figure B-3. Aerodynamic Heat Transfer Distributions at 0° Angle-Of-Attack

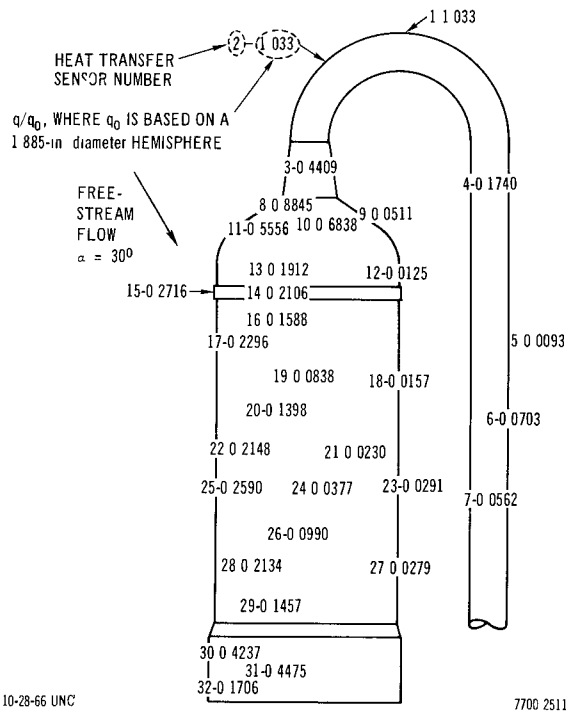

Figure B-4. Aerodynamic Heat Transfer Distributions at 30° Angle-Of-Attack

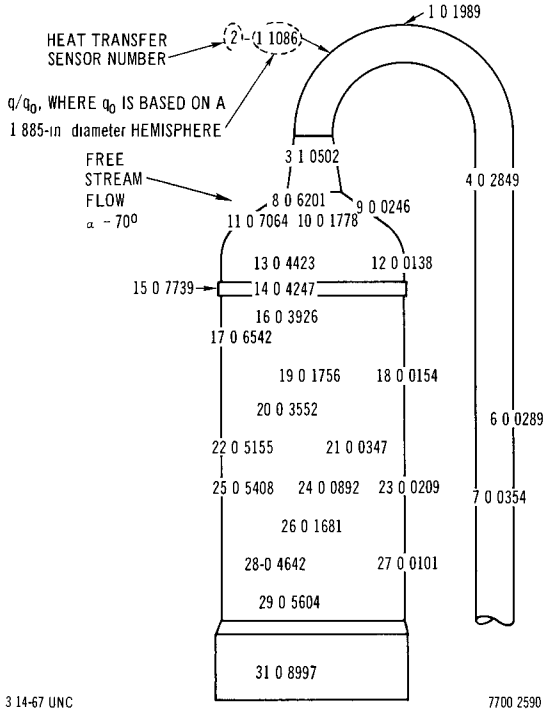

Figure B-5. Aerodynamic Heat Transfer Distributions at 70° Angle-Of-Attack

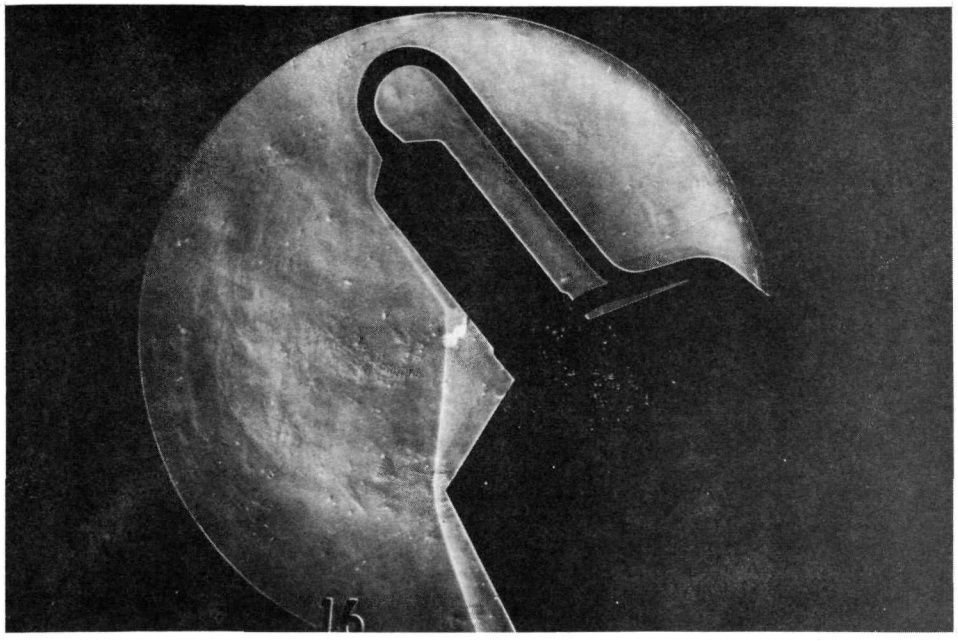

7-11-66 UNC 7611-2524

Figure B-6. Schlieren Photograph of Aeroheating Test Model

the vessel head at high angles-of-attack. This correlation discontinuity between 40 and 50° angle-of-attack is a result of the increased shock standoff distance at this location at high angles-of-attack. Evidence of this phenomenon is seen in the schlieren photograph (Figure B-6) taken at 50° angle-of-attack.

For the most part, the local heat-transfer distributions on the reactor head and vessel exhibit smooth correlations with angle-of-attack. The major flow separation influencing these data occurs at the low angles-of-attack where the forward piping and relatively blunt vessel head separate the flow from the vessel sides. The expected trend of higher heat-transfer rates with increasing angle-of-attack can be seen for all data in this area of the system. This is the result of each local body segment being translated to a position approaching normal with respect to free-stream flow with increasing angle-of-attack. A very minor perturbation to the flow is seen to result from the rib between the reactor vessel and head. The flow separates at the rib with a corresponding decrease in heat transfer at, and directly aft of the rib. The effect of the blunt shield has a pronounced effect on the flow field in the

vicinity of the reactor vessel. This can be seen graphically in Figure B-6 where the shock wave generated by the shield stands off by approximately 40% of the vessel length at 50° angle-of-attack.

To determine the local heating factors used in the 0, 30, and 70° angle-of-attack cases, a linear interpolation was made between the heat sensor locations on the Cornell aero-heating test model for each analytical node location.

Heat sensors 3, 8, 11, 15, 17, 25, 30 and 32 are located along the stagnation line of the test model. The length to these heat sensors were normalized to the overall length of the test model, which was taken as the distance from the base of the NaK outlet pipe to the top of the neutron shadow shield. The heating ratios for each case investigated were plotted at the corresponding normalized length as shown in Figures B-7, B-8 and B-9. The axial nodal locations on the analytical model were similarly normalized to the corresponding length on the analytical model. These normalized locations, for each angle-of-attack case, were superimposed upon the respective Cornell data trace. In this way, the local heating factors for each axial nodal location were read directly from Figures B-7, B-8, and B-9, and are given in Table 3.

D. CONCLUSIONS

The heat-transfer data derived from the Aero-heating test provides a relatively complete heat-transfer distribution over the SNAP-8 system configuration in the range of 0 to 70° angle-of-attack. The data have been normalized to the stagnation point value of a 1.885-in. diameter sphere for convenience. However, these normalized data can be converted to a 1-ft sphere reference through a multiplication factor consisting of a square root of the radii ratio. In addition, this is the method for determining the absolute heating rates to a system along a theoretical flight trajectory.

In the event that a heating investigation be undertaken for a reactor reentering free from the shield, care must be taken to use the forward and vessel heating distribution over the entire vessel. This is due to the flow field generated around the lower portion of the vessel as a result of the aerodynamically blunt shape of the shield.

The primary emphasis of the test was placed on acquisition of date free from a piping-dependent flow field. This was done on the premise that piping

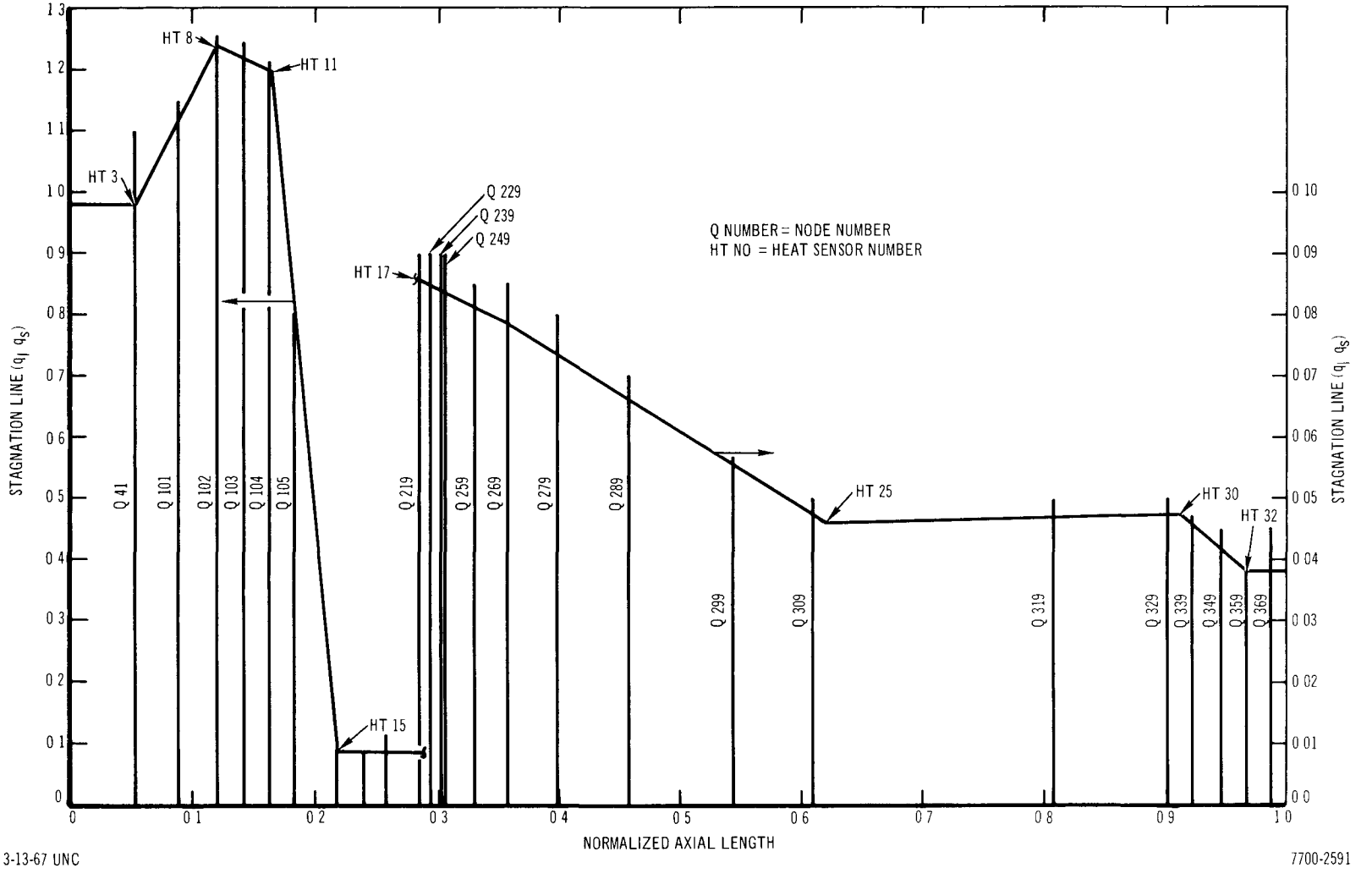

Figure B-7. Local Heating Factors Along Stagnation Heating Line (0° Angle-Of-Attack)

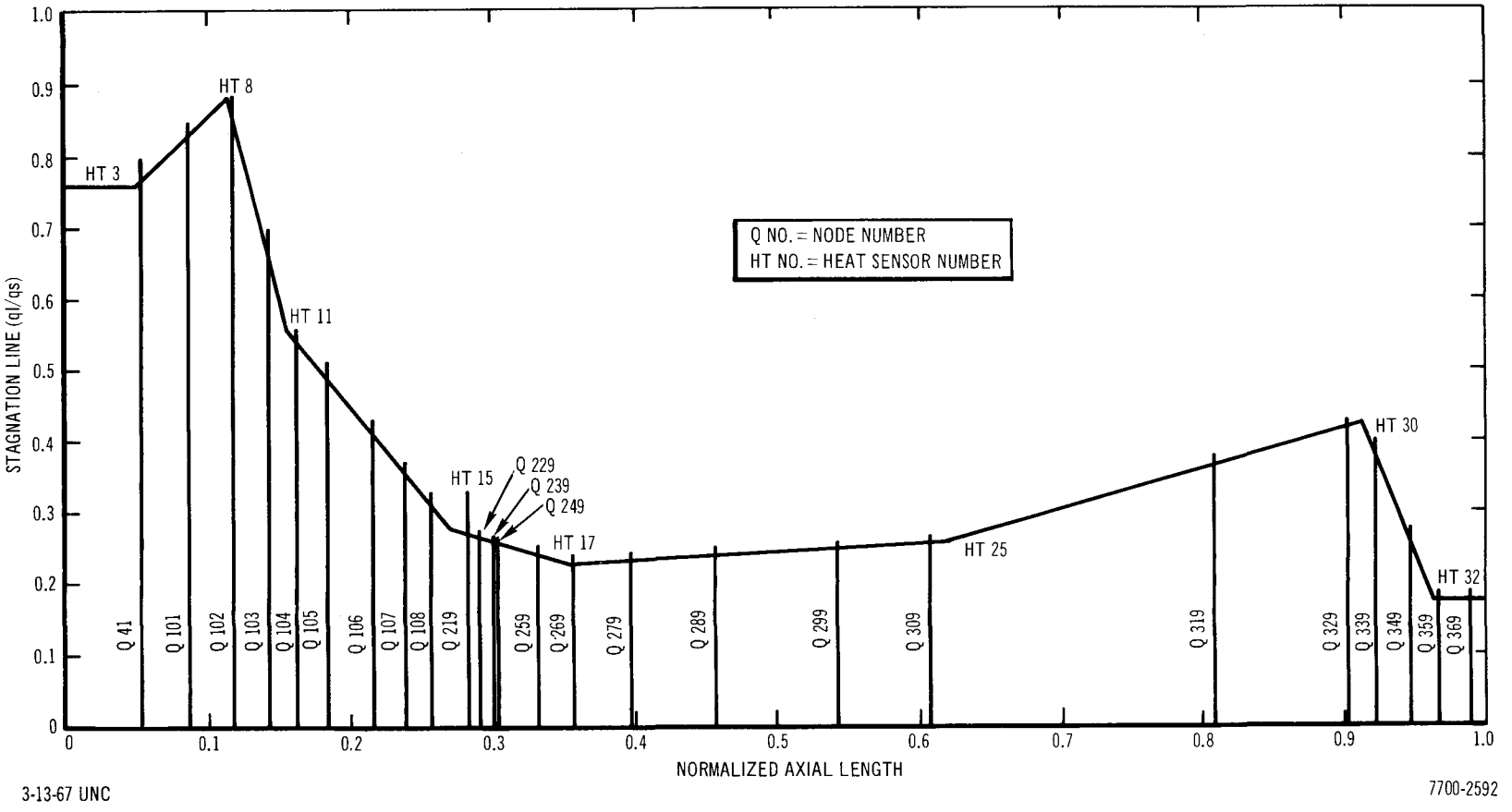

Figure B-8. Local Heating Factors Along Stagnation Heating Line (30° Angle-Of-Attack)

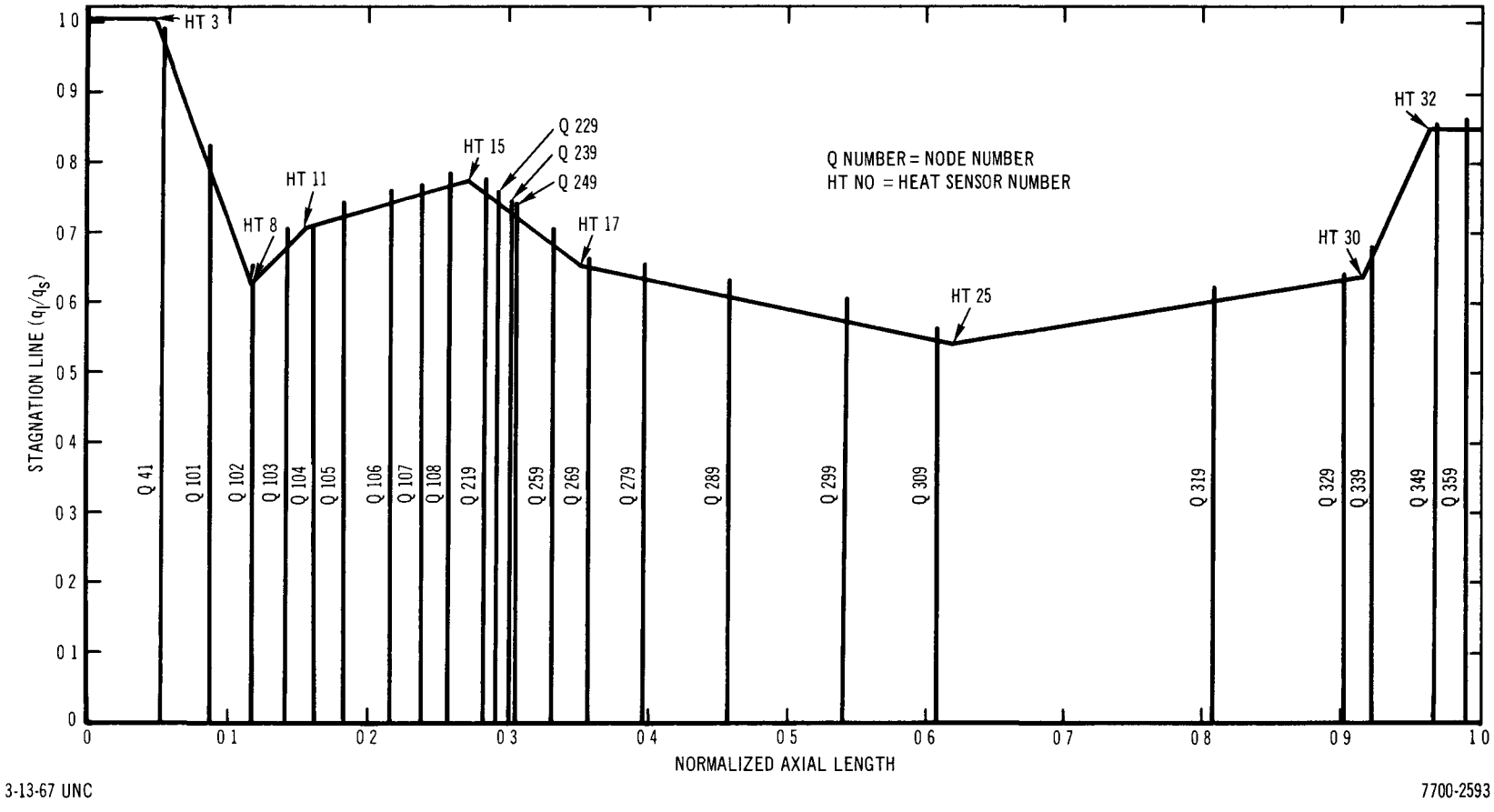

Figure B-9. Local Heating Factors Along Stagnation Heating Line (70° Angle-Of-Attack)

will undergo early ablation, and not contribute significantly to the overall heating received by the vessel. However, the test runs made at 30 and 60° angle-of-attack with piping directly in the flow should provide sufficient data to evaluate the thermal response of the piping to reentry heating.